DISTRIBUTION OF ICINGS (AUFEIS) IN NORTHWESTERN CANADA: INSIGHTS INTO GROUNDWATER CONDITIONS

By

Hugo Crites

Thesis submitted to the University of Ottawa in partial fullfillment of the requirements for the Master's of Science (M.Sc.)

Department of Geography

Faculty of Arts

University of Ottawa

Abstract

Icings, also known as aufeis, are groundwater fed sheet-layered ice bodies that normally forms in local depression or more often in low angled, shallow river beds. Understanding their distribution in the Mackenzie Valley corridor (N.W.T.) and adjacent Yukon (618,430 km^2) provided important insights to groundwater discharge and recharge. This study aimed at; i) creating the first extensive map of icings in Northwestern Canada, using over 500 late-winter scene Landsat 5 and 7; and ii) assessing hydrographic parameters (streamflow, baseflow and winter contribution) and terrain factors (slope, permafrost, geology) on icing distribution at the watershed level. Results show that; 1) icings are likely to develop close to geological faults on carbonate foothills and mountainous terrain, where continuous permafrost is present and on slopes of less than 5 degrees; 2) in the continuous permafrost zone, the cumulative surface area of icings, winter discharge and winter contribution to total annual discharge have significant positive relations with watershed extents. Icings located at the southern boundary of continuous permafrost are more sensitive to degrading permafrost and the predicted increase in groundwater discharge which may lead to a later icing accretion and earlier ablation during the year.

Acknowledgements

This thesis could have not been realized without the help of many individuals. First of all, I would like to thank my supervisor, Denis Lacelle, for providing me the opportunity to carry research under his supervision, for keeping me on track and providing invaluable comments on my writing as well as the thesis structure. I will keep good memories of fieldwork along the Dempster highway!

I could not go without mentioning Dr. Micheal Sawada for helping me making sense of my Python codes to iterate over my dataset. I cannot also forget the very helpful comments from my colleague and friend Benoit Faucher for help in R as well as Jean Bjornson from the Department of Geography for his insightful comments on my writing and figure design. Lastly, I could not got without mentioning the help and ongoing support from my partner Sheena and my parents, Ronald and Ginette.

Table of Contents

List of Figures

List of Tables

1. Introduction

Permafrost and hydrology are coupled components in many Arctic systems (Woo et al., 1992; 2008; Bense et al., 2012). In northwestern Canada and Alaska, the warming climate has led to an increase in active layer thickness and warmer permafrost (Burn and Kokelj, 2009; Pastick et al., 2015). The changing climate and degrading permafrost has been associated with several hydrological effects including a reduction in the area of ponds and lakes (Riordan et al., 2006; Labrecque et al., 2009), an increase in winter baseflow for many watersheds draining to the Arctic Ocean (Walvoord and Striegl, 2007; St-Jacques and Sauchyn, 2009; Walvoord et al., 2012), that, despite minimal changes to total annual discharge (Dery et al., 2005; McLelland et al., 2006). The changing permafrost and groundwater conditions may affect the formation of seasonal surface ice formed from groundwater such as icings, also known as naled or aufeis. These features provide critical habitats for overwintering of certain fish species, namely the Dolly Varden char (Mutch and McCart, 1974) and are a source of drinking water for some northern communities during winter months (Clark et al., 2001).

Icings, which are horizontal to sub-horizontal sheet-like ice mass, develop during winter on the ground surface by the freezing of successive flow of water that; i) seeps from the supra-permafrost (ground icings); ii) flow from a spring (spring icings) or; iii) emerge from below the river ice from the intra or sub-permafrost through fractures (river icings) (Carey, 1973; Sokovol et al., 1989; Pollard and Van Everdingen, 1992; Pollard, 2005). Icings have been reported in sub to high Arctic regions (Morse and Wolfe, 2015; Pollard, 2005), and also in mid-latitude mountainous regions (e.g. Three Forks, Montana; Stevens, 1940). Early studies on icings focused on their morphological characteristics (Carey, 1973; Kane, 1981), their development and energy

balance (Yoshikawa and *al.*, 2007), their seasonal and perennial contributions to fluvial regime (Clark and Lauriol, 1997), with more recent studies investigating the groundwater recharge sources (Clark and Lauriol, 2001; Utting et al., 2013). Irrespective of the source of groundwater within the permafrost, icings have a seasonal behaviour starting with the accretion of a basal icing layer in late fall/early winter, the successive freezing of a mixture of overflow water and snow in winter and the ablation of the ice in the spring that can last until mid to late-summer. In some instances, the combination of a sheltered location in the fluvial plain, low summer air temperatures and a substantial ice volume will allow icings to persist year-long (e.g. the Firth River aufeis in northern Yukon; Lauriol et al., 1991; the proglacial icing of Fountain Glacier, Bylot Island, Nunavut; Wainstein et al., 2014). Depending on groundwater recharge and winter conditions, the volume of ice stored in icings can vary from year to year. For example, Hu and Pollard (1997) reported ice volumes almost twice as high in 1992-93 compared to 1993-94 for the North Klondike aufeis on the Blackstone River. Given the strong linkage of icings with active groundwater system, insights on the response of these features under degrading permafrost and changing groundwater conditions may be gained by obtaining information on their historical distribution across the landscape, their surface area and changes ice volumes using a remote sensing approach.

This thesis investigates the occurrence of icings in the northwestern Canada since the 1980s and determine their link with groundwater conditions. The objectives of the study are to: 1) produce the first distribution map of icings in northwestern Canada; 2) determine the winter groundwater contribution to the total annual discharge of rivers in the study area (1970-2016); and 3) explore relations between the distribution of icings and winter groundwater conditions. The objectives

were reached by applying three indices to a dense stack of Landsat imageries (1985-2015) to identify icings, determine their extent and assess their connexion with precipitation, terrain and winter discharge conditions. The results will allow to predict the response of icing activities in the context of warming permafrost and changing groundwater conditions.

2. Background

2.1 River icings

River icings, one of the most common type observed, generally develops in streams and rivers (figure 1), especially in wide braided channels (Carey, 1973). Topographically-constrained, the extent of river icings with limited supply of water will generally not exceed the river channel boundary, while a continuous supply of water could result into icings extending onto floodplains and even reach the hills forming the valley sides (Lauriol et *al.,* 1991). Therefore, morphology and channel hydraulic conditions, especially low slope angle coupled with a wide and shallow profile, are important factor in river icing formation (Hu and Pollard, 1997).

The formation of river icings can be divided into three stages (Hu and Pollard, 1997); (1) "freeze-up", (2) "obstruction" and (3), "overflow". Initial ice accumulation starts in mid-to-late fall when air temperatures drop below 0 ^{o}C. Frazil ice starts to develop in the supercooled water and adheres to steam or river bank. This then initiates the formation of first layer of ice over the channel. When the streamflow is confined under this layer, hydraulic pressure increases, and water starts to emerge from cracks in the ice layer or at the interface of river bank and ice cover (Pollard and van Everdingen, 1992). Also, where the braided channels have larger shrub vegetation on the islands and banks, water can flow between the stem and ice interface due to the thermal conductivity difference between the two. The excess water can run over the initial layer and starts freezing in sheets that may range from less than an inch to a foot or more, depending on water input and air temperature. Thin overflows can travel tens of meters in distance before freezing, while greater overflows will flood further downstream. These overflow events can occur simultaneously at several points along the channel and the resulting layers might merge together into one large sheet. However, outpouring events can occur at several distant points

along the stream creating distinct icings (Carey, 1973). Caused by the gradual freezing of trapped water lenses, ice mounds are morphological features found on aufeis surface. Because river baseflow generally exceeds groundwater resurgence from springs or taliks, river icings are generally the largest type of aufeis observed (Carey, 1973). Depending on water input and winter conditions, icing volume can vary extensively from year to year; in the winter of 1993-1994, Hu and Pollard (1997) calculated approximate volumes of 6.10×10^5 m^3 and 7.10×10^5 m^3 for the Blackstone River and North Klondike aufeis, respectively. The volumes of 1992-1993 were almost twice of those observed in 1993-1994 (Hu and Pollard, 1997). Unless water input is limited, icing thickness will reach a maximum just before the melting season.

Although permafrost plays an important role in river icing formation processes, its occurrence is not always crucial (Pollard, 2005). Some observations about icings in northern Alaska by Kane (1981) revealed that permafrost was closer to the bed of rivers than the areas surrounding lakes in discontinuous permafrost. Additionally, the pore pressure was found to be greater on the river bank than further away from it. The primary water source of river icings comes from river baseflow, but contribution from surface runoff of adjacent streams and neighboring kettle lakes is also possible. Supra-, intra- and sub- permafrost groundwater may participate in river icing activity through taliks (Woo, 2012). The latter can be divided in 3 categories; (1) Closed taliks that form below lakes, river terraces and talus fans. The intra-permafrost horizons are connected to the supra-permafrost water which recharges the talik, (2) closed taliks where the intra-permafrost water is located in lenses without any contact with sub- or supra-permafrost water, or (3), open taliks that occupy extensive areas where sub- supra- and intra-permafrost waters are connected, unless flow is impeded by an impermeable strata. Found in mountain valleys and

fault zones where river icings can be located, these taliks are narrow and usually long, deep, alike a vertical crevasse. Their occurrence depends on the convective heat exchange below the riverbed resulting from the permeability of the alluvium. Strips of willow and poplar along river bed and flood plains are common surface vegetation features of such taliks (Woo, 2012). A typical late winter cross section of a river characterized by icing activity would reveal; (from top to bottom) snow cover, icing, initial ice cover, water, and stream alluvium (Kane, 1981).

Figure 1.The North Klondike River icing visible from the Dempster Highway, image taken on April 24th, 2016. Note the light blue icing ice (credits: Bernard Lauriol).

Figure 2. River icing in Erdaogou on the Tibetan Plateau during the spring. Note the surface ablation and maximal extent shown by trim-line of tundra vegetation on river banks. From Woo (2012).

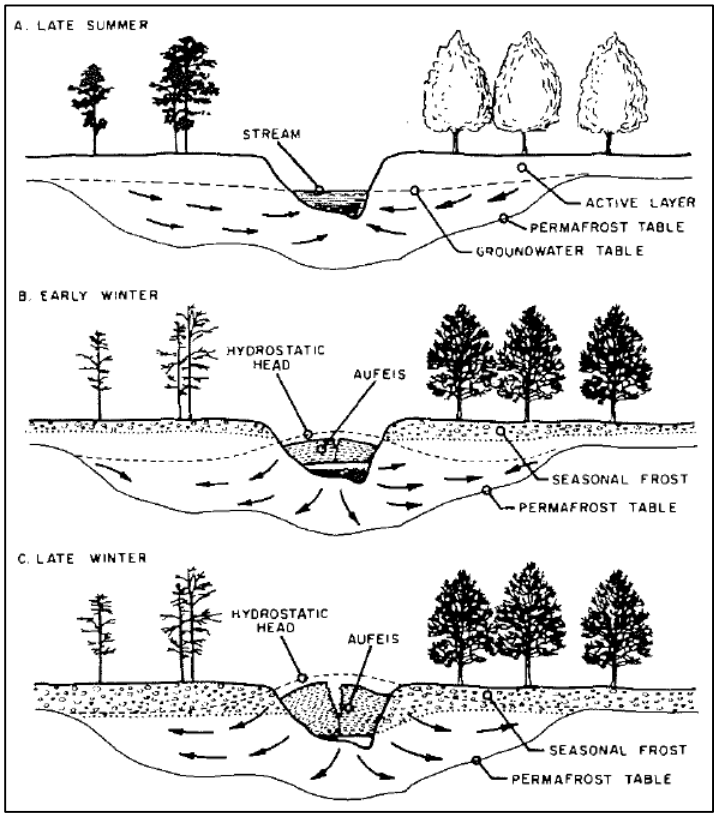

Figure 3. Schematic diagram showing groundwater flow pattern adjacent to stream with icing activity (modified from Kane, 1981).

2.2 Spring icings

The primary source of water that forms spring icings is from groundwater springs. Normally, the latter must flow sufficiently during the summer season to allow formation of well-defined channels where the groundwater reaches the surface (Carey, 1973). Extremely low air temperatures and limited discharge can limit spring icing formation close to water outlet. If higher water temperatures and discharge rates occur, icings can form further from the point of discharge. If sub-permafrost groundwater is the only input (e.g. in continuous permafrost regions), discharge commonly stops before the end of winter, when reserves decline or conduits are frozen shut (Pollard, 2005).

Groundwater can exploit voids in the active layer and channels under the icing until the flow is restricted, which typically happens once air temperatures fall below the spring's freezing point. The growth of seasonal frost mounds beneath and around icings are typical features associated with this impeded flow. If frost mounds located below icings do not show irregular topography on the latter, this means they formed prior to icing activity (Pollard et *al.,* 1999). If substantial hydraulic pressure forms in icings, blisters can form and break, where artesian flow creates fountains that discharge until reserves are consumed.

Spring icings can also be linked to highly mineralized perennial spring activity from salt diapirs, like icings found at Gypsum Hill in Expedition Fjord, Axel Heiberg Island (e.g. Pollard et *al.,* 1999). Water inputs can have various sources; geothermal activity (e.g. Pilgrim, Alaska), meteoric water from surface runoff, ancient sub-permafrost groundwater, meltwater from warm-based glaciers or surface water bodies (e.g. nearby lakes) (Pollard et *al.,* 1999). Taliks can act as conduits between surface lakes and sub-permafrost groundwater, they are unlikely in areas of deep (>450 m) continuous permafrost (e.g. Axel Heiberg Island). Despite the low air

temperatures, significant freezing-point depression created by dissolved salts in spring water permits discharge in environments well below -20 ^{o}C (Omelon et *al.,* 2005). Freezing fractionation contributes to raise solute concentration in the remaining spring discharge, which further depresses the freezing point (Pollard, 2005). However, snow cover can effectively dilute spring solute concentration and allow icing formation at higher temperatures (Pollard, 2005). Formation of relatively pure ice normally occurs close to spring discharge while "salty ice" (i.e. ice that forms when temperatures are close or below the eutectic point) is found further away from the outlet. Following freezing-point depression experiments, Pollard (2005) recognized that hydrohalite ($NaCl{\cdot}2H_20$), a mineral metastable at low temperatures, crystallizes out of solution and is integrated within the ice structure. In this case, the term ''brine icing'' would be used to refer to such ice. Typical paste-like gypsum residue can accumulate on icings, resulting from evaporative fractionation of spring outlet (Pollard et *al.,* 1999). When the icing melts, the paste is reduced to a fine powder as it dries, which is then removed by surface runoff during the summer.

Different discharge rates, temperatures, dissolved minerals and topographic settings are factors contributing to the considerable variation of icing processes. Monitoring spring icings in Expedition Fjord on Axel Heiberg Island since 1989, Pollard et *al.* (1999), noticed varying shapes, thicknesses and extents (e.g. surfaces ranging from 300 000 m^2 in 1989 and 120 000 m^2 in 1995). The observed variable icing extent could be explained by yearly differences in melt processes and the period at which they were observed.

2.3 Ground icings

Ground icing, also defined as “seepage” icing (Carey, 1973), results from limited groundwater surface seepage. Unlike spring or river icings, they usually develop in poorly defined area; topographic lows that are merely saturated by groundwater during summer. Their relative small size is controlled by the supply of feeding groundwater, which is usually limited and becomes exhausted before melt season. Spring icings are usually larger because of the continuous feed of deeper groundwater. Ground icings can take various shapes; from flat to slightly arched, they can also be found on steep slopes and form an icefall (Woo, 2012). Growth surges are possible following thaw, as water can collect because of topography and refreeze at night (Carey, 1973). Those seeps are slow surface discharge of water from the ground via voids and cracks in unconsolidated material, fissures and bedding planes in rocks (Woo, 2012). They can also occur underwater and discharge directly into streams and rivers. If the groundwater source is saturated in organic material, a noticeable reddish-brown hue appears on icing surface (Figure 4). These seeps can be supplied by sub-permafrost groundwater where the water table intersects the ground surface (Woo, 2012).

Figure 4. Reddish-brown colored ground icing at the base of a concave slope east of Teller (Woo, 2012).

2.4 Ice characteristics

The ice formed in icings can be dry, wet or slushy (following a snowfall), depending on icing activity at the given time. Mostly flat, terraces can form following thin overflows, showing edges of recent frozen layers. Cracks can develop from the expanding of ice mounds formed by freezing of unfrozen water lenses. In general, the ice usually is clear but can also be white as a result of the entrapped air bubbles. In some cases, a faint yellow or tan color can be observed within the ice structure, which is caused by the presence of dissolved salts or organic material in the source water (Akerman, 1980). For example, isotopic analysis of cryogenic calcite precipitates found within the structure of the Firth River aufeis in northern Yukon, indicated that karst groundwater was the principal water input (Clark and Lauriol, 1997). A cross-section of an aufeis could reveal voids (empty blisters), porous ice, layers of needle ice, or small water layers near the surface.

2.5 Geotechnical concerns

Icings have been recognized to cause certain issues for road infrastructures in Alaska and Yukon since the 1930's (Sterling, 1935; Taylor, 1939). During World War II, roadways such as the Alaska Highway, the Yukon Highway 6 (formerly known as "Canol Road") and the Glenn Highway, were built and were accessible year-round rather than only during summer months. Man-made constructions such as culverts, bridges, raised roadbeds, pipelines would increase water pressure upslope, creating conditions favorable to icing formation. An example of a larger culvert to accommodate icing is shown in Figure 5b. Common culvert obstruction is shown in Figure 5a, where holes on the top of culverts are used to inject steam and thaw icings.

Given the increase in road infrastructures in Arctic Canada, road planning officials are interested in knowing the distribution of icings, especially with the all-season road project (Mackenzie Valley Highway) linking the community of Wrigley with Inuvik, N.W.T.

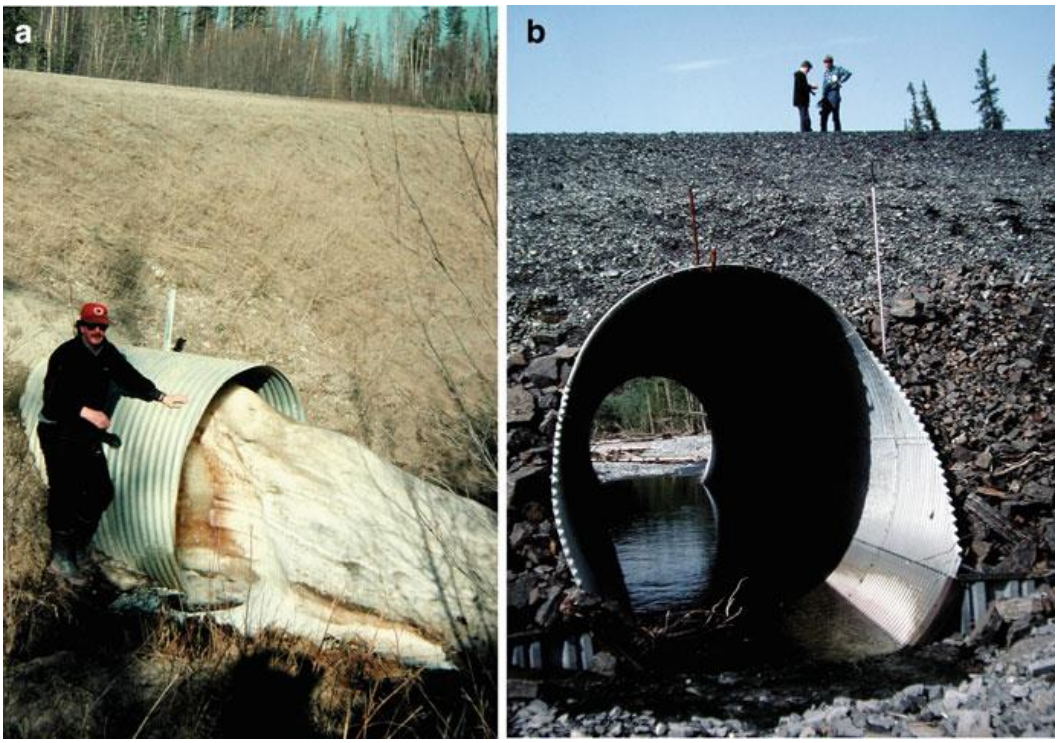

Figure 5. Icing in discontinuous permafrost area: (a) Terry Prowse standing next to a small culvert choked with icing, Fort Simpson, NWT. (b) Large culverts installed at a river crossing of the Dempster Highway to accommodate icing (from Woo, 2012)

2.6 Mapping of icings

Icings have been of general interest to the scientific community for a long time and were initially mapped from aerial photographs, ground photos and field observations (Akerman, 1980; Bukayev, 1973; Nekrasov, 1969; Hall and Roswell, 1981; Dean, 1984; Lauriol, 1991). Their identification in the landscape by various remote sensing techniques are limited to their surface area. The extent of icings can vary from several 100 m^2 on gently sloping terrain to over tens of km^2 in river valleys. Ground icings fed by supra-permafrost water will generally reach much smaller surface area than spring icings, where sub-permafrost water can continuously discharge

during the winter months. River icings, supported by higher groundwater discharge (baseflow) than spring and ground icings, are typically much thicker and larger (Woo, 2012). Carey (1973) quoted that an icing observed in the Moma River valley (a tributary of Indigirka River in Siberia), had a length of 25 km and a width up to 8 km.

Harden et *al.* (1977) and Dean (1984) conducted the first thorough mapping of icings from satellite imagery on the northern slope of Alaska using Landsat-1 MSS and aerial imagery. They manually delineated icings by selecting images from bands 4 and 5 (green and red, respectively) where contrast between icings and the surrounding tundra and exposed bedrock was clear. Images from band 7 were also used to map late-winter overflows due to absorption of water in those wavelengths (Dean , 1984). Fortunenately, optical imagery with higher resolution from spaceborne sensors like Landsat 5, 7 and 8 are now available.

Morse and Wolfe (2015) used Landsat TM, ETM+ and OLI imagery to develop a semi-automated method to identify icings in the Great Slave Region around Yellowknife, Northwest Territories, a region close to our study area. Their approach consisted of using Landsat 5, 7 and 8 late-spring images and a series of three spectral indices to achieve icing classification: (1) Normalized Difference Snow Index (NDSI), (2) Maximum Difference Ice Index (MDII) and, (3) Normalized Difference Water Index (NDWI). The NDSI and MDII were applied on the late-spring imagery to identify icings. The NDWI was done on a separate stack of summer images to create a water mask. The NDSI classified all snow, water and ice from the image against soil and exposed bedrock. To extract ice from snow and water, they used the MDII to map iced

pixels on the imagery. As a final step, a water mask removed other frozen freshwater bodies such as lakes and rivers in order to map icing ice only.

More recently, Pavelsky and Zarnetske (2017) used the Moderate Resolution Imaging Spectroradiometer (MODIS, 250m pixel resolution) to create a daily time-series to show temporal persistence and minimum summer time extent of large river icings in the north slope of Alaska. To calculate icing surface, they used an automated method for thresholding of MODIS band 1 (620-670 nm). An initial surface reflectance threshold value of 0.15 was selected, while also trying 0.20 and 0.10, to notice no significant change in overall icing feature size within this range of pixel values. Selection of icings for analysis was based on previous known occurences and icing size so that they appear on the imagery (extent > 0.25 km^2). Icings sufficiently distant from other commonly ice-covered features were also preferred to avoid wrongful classification.

The use of synthetic aperture radar (SAR) and optical imagery has been used by Yoshikawa et al. (2007) to assess surface water conditions and icing surface in the Brooks Range, Alaska. An advantage of SAR imagery (ERS-1, ERS-2 and RADARSAT) is that temporal series can be easily created because of the relatively short revisit time of the spaceborne sensor, regardless of cloud-cover. Icing delimitation was done by using radar backscatter properties of water, ice and the surrounding tundra to establish thresholds for classification. The C band (5.3GHz) thresholds were done 181 images that were acquired between April 1996 and September 2005. Threshold values varied with the time of year the image was acquisitioned; -18 dB for images without snowcover and -8 dB for snow-covered scenes. Contrast between icing surface and the surrounding tundra was clear in the summer images, but less clear during winter months where

snow covered most of the ground. Difference in surface roughness and wetness permitted to better identify icings on winter SAR imagery. As radar backscatter is affected by surface ruggedness and wetness, the irregular icing appeared clearly against the smooth surrounding snow cover. Spring discharge on icing surface created a contrast in ground wetness that was identifiable on the imagery. However, pixel values for inundation events from high spring discharge fell below the threshold and were included in total aufeis area (Yoshikawa et *al.* 2007).

3. Study Area

The study area in northwestern Canada ranges from 62 to 69°N and from 118 to 140°W; covering a surface area of approximately 618,430 km^2 (Fig. 1). Elevations range from sea level along the Beaufort Sea coastline to 2919 m.a.s.l. in the Mackenzie Mountains, with 50% of the study area located below 400 m.a.s.l.. A total of 28 ecoregions are found within the study area; the northern sector includes mainly flat terrain (Mackenzie Delta and various plains), rolling hills (Peel Plateau) and also includes the Richardson and Brooks mountain ranges, whereas the southern sector includes more mountainous regions like the Mackenzie and Ogilvie Mountains. The surficial geology is quite varied with mainly glacial deposits in glaciated regions and colluvial deposits at the bottom of hillslopes and also on the steeper valley walls in the mountainous regions (Aylsworth et *al.*, 2000). Vegetation ranges from tundra in the northern plains and mountainous regions to boreal forest in the southern region. Wetlands and peatlands are also common features in poorly drained lacustrine sediments (Zoltai *et al.*, 1988).

Table 1. Ecoregions in the study area (Ecosystem Classification Program, N.W.T. Environment and Natural Resources, 2014).

Ecoregion	**Area (km2)**	**Ecoregion**	**Area (km2)**
Anderson River Plain	402	Mackenzie River Plain	16240
Tuktoyuktuk Coastal Plain	32672	Mackenzie Mountains	87025
Yukon Coastal Plain	1491	Franklin Mountains	6702
Dease Arm Plain	14067	Keller Lake Plain	13385
British-Richardson Mountains	13792	Klondike Plateau	11937
Mackenzie Delta	9234	Yukon Plateau-North	29500
Old Crow Basin	2492	Selwynn Mountains	54253
Great Bear Lake Plain	77098	Great Slave Lake Plain	5404
Peel River Plateau	60324	Yukon Plateau-Central	2013
Colville Hills	17259	Horn Plateau	10194
Fort MacPherson Plain	30405	Hay River Lowland	5457
Eagle Plains	17892	Sibbeston Lake Plain	555
North Ogilvie Mountains	21113	Liard Basin	462
Norman Range	42575	Nahanni Plateau	599

3.1 Climate

The climate in the study area is characterized by a subarctic climate regime (Dfc), with cold winters and cool summers. Climate data from nine Environment Canada weather stations show a latitudinal gradient in mean annual air temperature (MAAT) for the period 1980-2010. Stations in the southern sector have the warmer MAAT, with values ranging between –0.7 and 0.8°C; whereas the northern stations have MAAT ranging between –10.4 and –10.5°C. Since 1980, the northern region experienced a warming trend of 0.05 to 0.1°C yr^{-1}, whereas the more southern region experienced a warming of 0.002 to 0.05°C yr^{-1} (Fig. 7). Total annual precipitation across the study area range from 240 to 450 mm (Environment Canada). Based on the 1979-2007 blended precipitation dataset (CanBPv0; Lin and Wang (2011)), precipitation in the study area is greater in the southern region and decreasing toward the Beaufort Sea. Zhang et al., (2000) reported increased precipitation in NWT for the 1950-1998 period due to increase in snowfall. However, since 1980, no consistent spatial trends in total precipitation is observed across the study region, with some stations showing a decreasing trend (–1.1 to –0.76 mm yr^{-1}) and others showing an increasing trend (0.02 to 2.5 mm yr^{-1}).

Table 2. Comparison of yearly precipitation average of Environment Canada precipitation normals and results from the blended precipitation dataset CanBPv0 (see section 4.4).

Weather station	**CanBPv0 (1979-2007) (mm)**	**Environment Canada normal (1981-2010) (mm)**
Norman Wells	285	295
Mayo	360	313
Old Crow	275	279
Inuvik	238	240

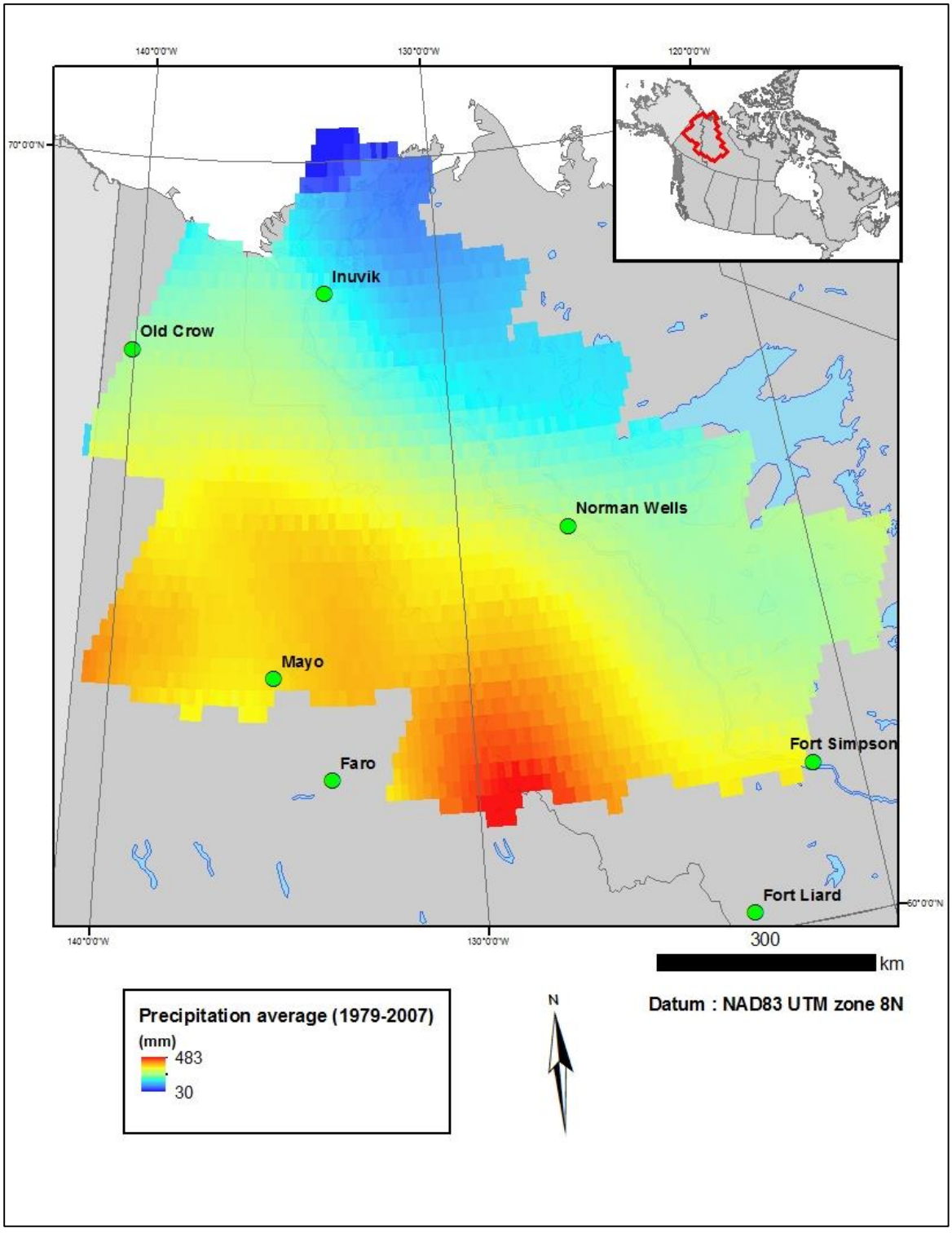

Figure 6. Map showing the 1979-2007 yearly precipitation average from CanBPv0 blended precipitation dataset. Note, this dataset has a half degree (both x and y) spatial resolution.

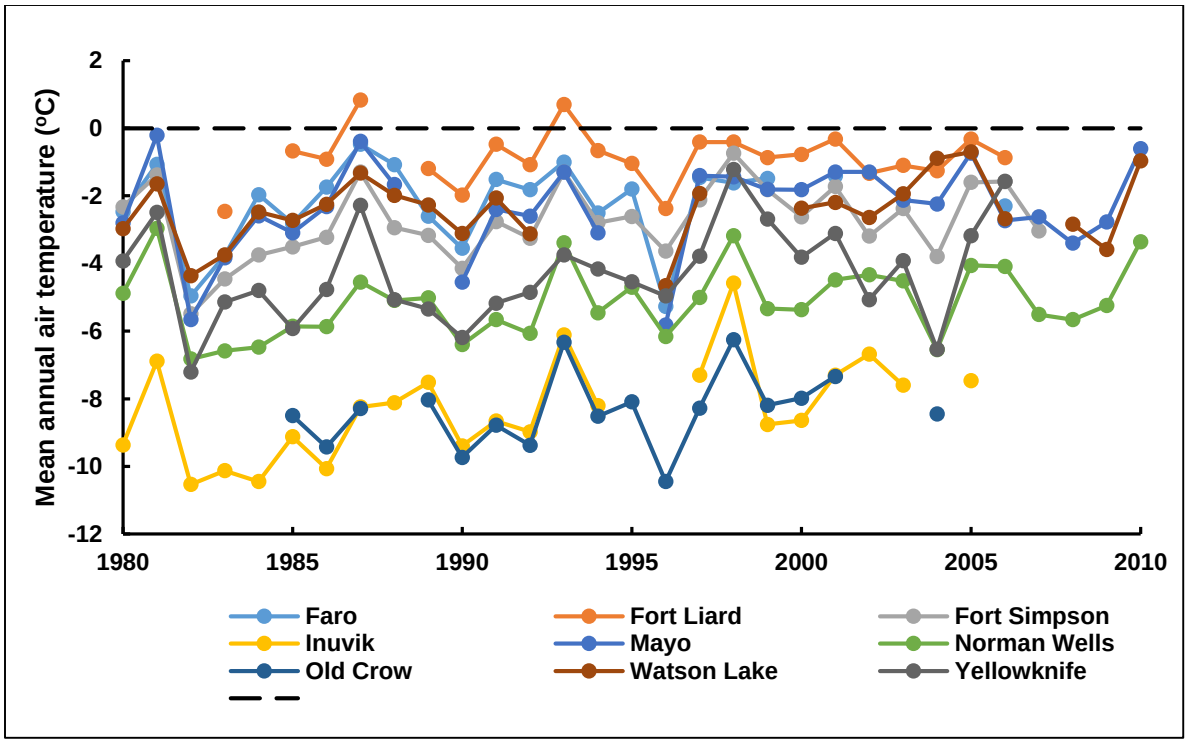

Figure 7. Graph showing mean annual air temperatures for the selected weather stations.(Environment Canada)

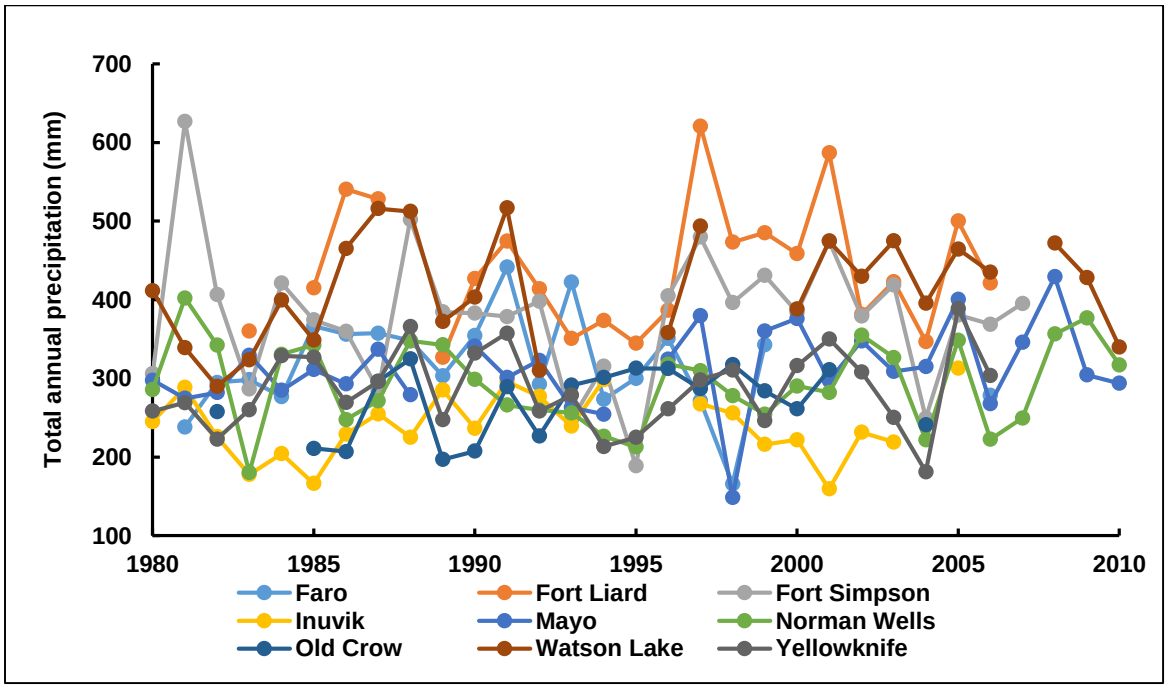

Figure 8. Graph showing total annual precipitation for the selected weather stations.(Environment Canada)

3.2 Permafrost

The climate and vegetation conditions ensures that permafrost is continuous in the northern plains and mountainous regions. Extensive discontinuous permafrost occurs at lower latitudes and elevations. (Figure 9). The Circumpolar-Active-Layer-Monitoring (CALM) program has 13 sites along the MVC where the active layer thicknesses (ALT) was monitored from 1987-2001. A general reduction in active layer thickness was observed with increasing latitude, ranging near 200 m at the southern section to near 50 cm in the north (Nixon & Taylor, 1998; Burn and Kokelj, 2009). Interannual variation in ALT is greater than in ground temperature measurements. Compared to the 10-year mean (2003-2012), ALT increased since 2008 and exceeded the mean in 2009 and reached a maximum in 2012 (Smith et al., 2017). However, one of the maximum ALTs observed was during 1998, one of the warmest years on record (Duchesne et al., 2015). Recent increases in ALTs are likely in response to rising air temperatures (Smith et al., 2017).

Borehole data (2013-2015) of mean annual ground temperatures (MAGT) measured at the depth of zero annual amplitude in the discontinuous permafrost zone are generally above -2°C with slightly colder conditions at the fringe of the discontinuous and continuous permafrost zones (~-2.5°C; Smith et al., 2016). In the continuous permafrost zone, the pemafrost is colder at sites around Inuvik (-4°C) and lower than -6°C at tundra upland sites. Permafrost temperatures between 2007 and 2015 along the Norman Wells and Fort Good Hope corridor (64 to 66°N) showed an increase of 0.03°C y^{-1} and sites between Norman Wells and Wrigley (63 to 64°N) showed an increase less than 0.02°C y^{-1} (Smith et al., 2016).

3.3 Hydrology

The study area includes 55 level-three watersheds and most of the rivers are characterized by sub-arctic to arctic nival flow regime. Gauging records of 23 rivers in NWT showed that winter baseflow contributes 1.2-87% to the total annual discharge, with the majority (20 out of the 23 stations) experiencing an increase in baseflow contribution (0.5-271% yr^{-1}) over the 1977-2007 period (St-Jacques and Sauchyn, 2009). Similar observations were made for 21 gauging stations in the Yukon River basin, where groundwater contributed 4.7-47.4% of the total annual discharge and with an increase of 0.4-2.6% yr^{-1} between 1949 and 2005 (Brabets & Walvoord, 2009; Walvoord & Striegl, 2007). It was suggested that the low-lying areas underlain by continuous permafrost receive >10% of groundwater contribution to their annual flow and the increase in groundwater contribution was attributed to permafrost degradation in response to warming air temperature (Walvoord and Striegl, 2007).

The presence of permafrost largely restricts groundwater recharge, except where fractured bedrock, sinkholes or dissolution channels are exposed at the surface (Michel, 1977; Van Everdingen, 1981). In the central Mackenzie Valley (Smith Creek, White Sand Creek and Gayna River) and northern Yukon (Fishing Branch and Firth River) groundwater is recharged from a mix of snowmelt and rainfall through saturated organic soils with no advection of heat to the subsurface (Utting et al., 2012). A similar recharge system has also been described for the North Klondike watershed in YT (Lapp et *al.*, 2017). Based on noble gas and isotope geochemistry, groundwater circulation times in the study area were found to be in the order of two to three decades (Utting et *al.*, 2012). The groundwater mostly discharge through overburden but direct discharge via fissures in exposed bedrock and talus has been observed where bedrock units intersect the surface due to folding or if the unit is intersected by a fault. Although folding is the

predominant structural style in the Mackenzie Mountains, thrust faults remain important for groundwater flow (Michel, 1986).

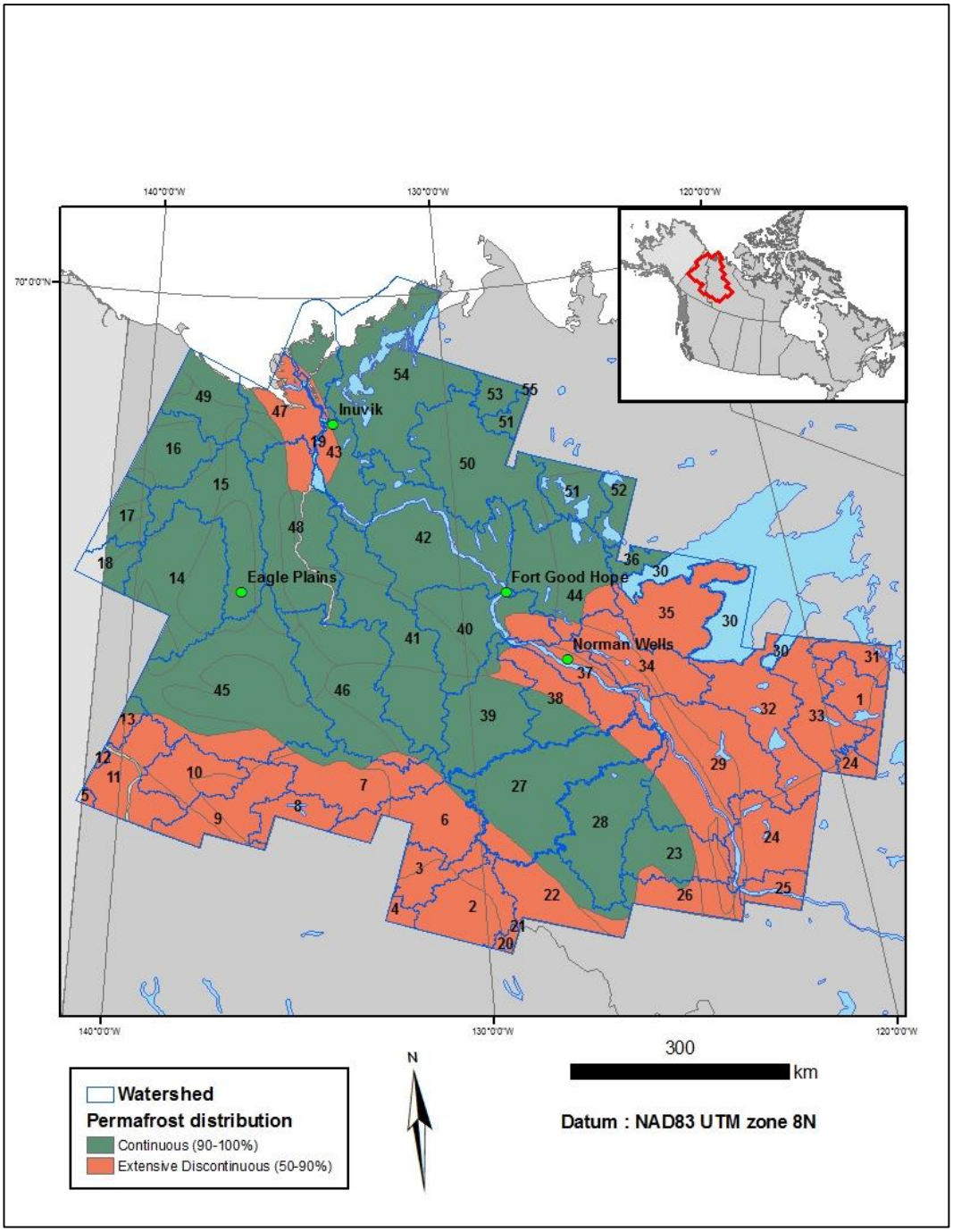

Figure 9. Map showing watersheds and permafrost distribution in the study area (data from the National Hydro Network, 2014)

Table 3. List of the different level-3 watersheds in the study area with corresponding numbers found on figure 9.

Watershed name and number (National Hydro Network)			
La Martre	1	Central Mackenzie - Blackwater	29
Upper Pelly	2	Great Bear Lake	30
Macmillan	3	Great Bear Lake - Camsell	31
Lower Pelly	4	Great Bear Lake - Johnny Ho	32
Lower White	5	Great Bear Lake - Johnny Ho	33
Hess	6	Great Bear - Mouth	34
Beaver (Y.T.)	7	Great Bear Lake - Northwestern	35
Upper Stewart	8	Great Bear Lake - Northwestern	36
Lower Stewart	9	Central Mackenzie - Little Bear	37
Klondike	10	Carcajou	38
Central Yukon - Sixty Mile	11	Mountain	39
Fortymile	12	Central Mackenzie – Ramparts	40
Central Yukon - Tatonduk	13	Arctic Red	41
Headwaters Porcupine	14	Lower Mackenzie - Ontaratue	42
Upper Porcupine - Bell	15	Eastern Mackenzie Delta	43
Old Crow	16	Hare Indian	44
Central Porcupine - Coleen	17	Upper Peel	45
Lower Porcupine - Mouth	18	Central Peel	46
Great Bear Lake	19	Lower Peel and Western Mackenzie Delta	47
Frances	20	Lower Peel and Western Mackenzie Delta	48
Hyland	21	Southwestern Beaufort Sea (YT)	49
Upper South Nahanni	22	Carnwath	50
Root	23	Upper Anderson	51
Upper Mackenzie - Willowlake	24	Upper Anderson	52
Upper Mackenzie - Martin	25	Lower Anderson	53
North Nahanni	26	Southern Beaufort Sea – Eskimo Lakes	54
Keele	27	Horton	55
Redstone	28		

4. Methodology

4.1 Landsat dataset

To produce the first extensive map of the distribution of icings in northwestern Canada, 573 level-2 Landsat scenes (31 path-rows) acquired from USGS (https://earthexplorer.usgs.gov) and USGS ESPA level-2 (https://espa.cr.usgs.gov) were used for analysis; a total of 27 Landsat footprints covered the study area (fig. 10). All images selected had a low cloud coverage (≤ 20 %) and were acquired by the sensor between May 1st and June 30th between 1984 and 2015. The late spring- early summer corresponds to a period when most of the snow melted from the landscape and icings are then more easily identifiable on the imagery. Scenes acquired in July were not considered since the extent of icings could be partially or completely reduced by melt. The Landsat archive was visually inspected because the Landsat's ACCA algorithm (Automatic Cloud Cover Assessment) does not always properly calculate cloud cover in scenes with snowy features (Foga and *al.*, 2017). For example, some images were assigned by the ACCA a cloud cover of 40% (which would normally be unacceptable) but after visual inspection, the imagery was useable. The selected imagery is listed in **appendix A**.

The Landsat 5 TM images provided about two thirds of the dataset and Landsat 7 ETM+ images were used to fill-in the gaps where no late-spring, near cloud-free images were available from Landsat 5. However, images acquired by Landsat 7 after May 31st 2003 have data gaps was caused by a failure of the Scan-Line Corrector (SLC), but are still useful as radiometric and geometric accuracy has been kept by the sensor. Gap-filling techniques exist (e.g. Zhu et *al.*, 2012), but as icing extent is spatially and temporally variable, SLC-off images were processed as is.

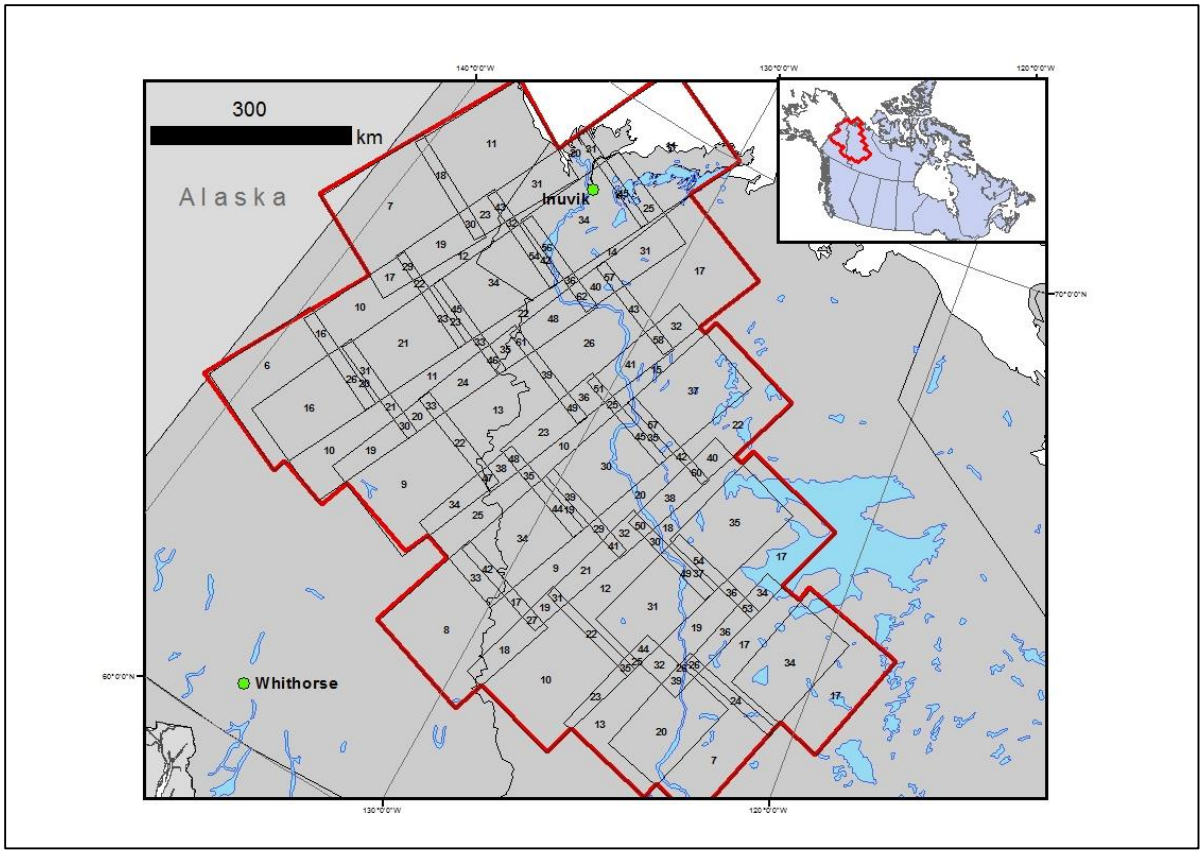

Figure 10. Map showing the overlay of the Landsat extent with the number of scenes selected labeled in center.

4.2 Image pre-processing

Passive optical remote sensing is confined by the laws of optical physics, where target reflectance properties, the position of the sun relative to the sensor, interactions (absorption and scattering) with the atmosphere constituents (aerosols) are parameters influencing the energy received at the sensor. Thus, multiple pre-processing steps are required to convert the raw data recorded by the sensor, to meaningful units that can be compared between scenes. Surface reflectance products (L2T) were used to account for the possible anisotropy in reflectance distribution created by large and mountainous areas and this level of product is necessary when conducting temporal studies in mountainous regions (Colby, 1991; Young et *al.*,2017). As the L2T products are available on-demand, all the selected L1T scene identifier (ID) were submitted

to the USGS Earth Resources Observation and Science (EROS) Center Science Processing Architecture (ESPA) via their on-demand interface. Scenes are processed by the ESPA facility and are then downloaded via the *espa-bulk-downloader* operated in MS-DOS command window.

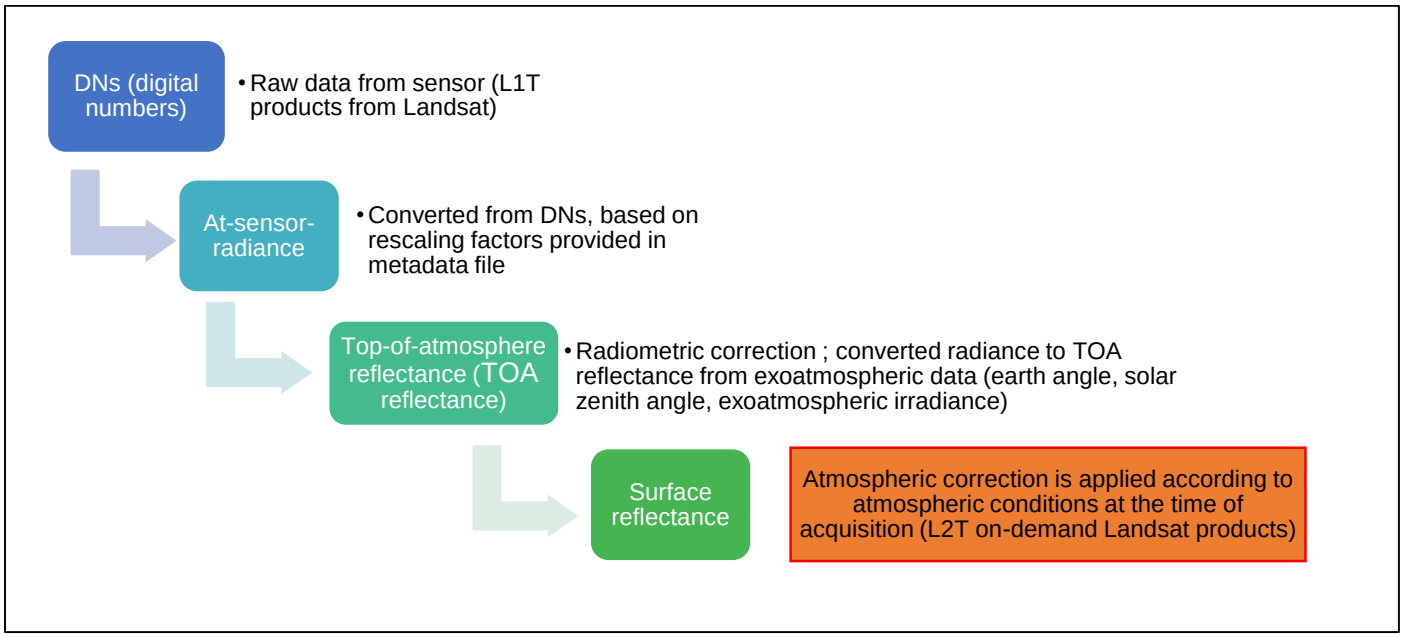

Figure 11. Diagram showing the various Landsat pre-processing steps.

4.3 Identifying icings from Landsat images

The methodology (figure 12) uses a dense stack of Landsat 5 TM Landsat 7 ETM+ imageries and follows a semi-automated approach established by Morse and Wolfe (2015) around Yellowknife (N.W.T.) but modified and adapted to the study area with varied physiographic characteristics. The mapping was done in ArcGIS 10.6 with *Python* (version 2.7) scripts (**Appendix B** provides the Python codes to process imagery). For all Landsat L2T scenes, we first calculate a Normalized Difference Snow Index (NDSI) that discriminates snow, ice and water from bare soils and clouds (Dozier, 1989):

1. NDSI = (Green – SWIR) / (Green + SWIR) (Dozier, 1989)

From the NDSI, Hall et *al.,* (1995) suggested that a surface reflectance threshold value of >0.4 identified ice, snow and water, whereas values <0.4 represented bedrock and bare soils. When exploring the resulting raster compared to a natural color composite, that threshold was accurate in selecting ice, snow and water. The product of this index is a binary raster (0 and 1), where pixels with a value of 1 indicate snow, ice and water; values of 0 include bare soil, bedrock and other components.

The Maximum Difference Ice Index (MDII) was then used on the thresholded-NDSI data to differentiate ice, water, snow and wet marl:

2. MDII = (Green – SWIR) (Green + SWIR) = ($Green^2 – SWIR^2$)

As we used L2T products, a rescaling factor of 0.0001 was necessary to obtain values between 0 and 1; (Vermote et al., 2016). After a visual inspection of a natural composite, a surface reflectance threshold value of 0.144 (Morse and Wolfe, 2015) was used to separate ice from snow and wet marl.

Following these two steps, late-lying snowbanks at higher elevation in the Mackenzie Mountains, the Ogilvie Mountains, British-Richardson Mountains and the Selwynn Mountains were still being classified as ice. Here, pixel values of ice (MDII) and late-lying snow (NDSI) were similar, making the separation using these indices impossible. The snowbanks at high elevation were removed from the classification by creating a Topographic Position Index (TPI), a measure of terrain ruggedness and local elevation index, that defines hilltops, slopes and valley bottoms. After visually inspecting the TPI output, values between < -5 and >+5 corresponded to

convex topographic features, which were used to mask late-lying snow on hilltops. The approach was successful in removing most of the snow; however, snow still remained along some slopes (mainly north-facing slopes) and elevated plateaus. As icings tend to develop in valley bottoms along stream/river channels (Carey, 1973), we explored different slope masks to remove these snow patches; the most effective slope angle was 30 degrees. Thus this value was used to mask slopes above this value. Following the application of the TPI and slope mask, mainly late-lying spring to early summer ice remained on the imageries (Figure 13). Nonetheless, some noise still remained and had to be manually inspected.

The classification included all ices present in the scenes (i.e. lake and river ice and icings). The lake and river ice was removed using a Normalized Difference Water Index (NDWI) from mid-summer cloud-free scenes (McFeeters, 1996):

3. NDWI = (Green – NIR) / (Green + NIR)

Pixels classified as water were digitized into polygons shapefiles using the *Raster to Polygon* tool (Figures 14 and 15). However, multiple braided rivers are present in the mountain ranges located west of the Mackenzie River and these can contain icings. Therefore, the NDWI was only applied to the flatter area east of the Mackenzie River (i.e., Canadian Shield). In addition, topographic shadows were being classified as water bodies by the water index. Figure 15 shows masking steps in an area where no shadows were created by topography and where the water bodies are clearly identifiable from the true-color composite. Figure 14 shows how shadows from topography are included in water classification; pixel values in the NIR band and green

band for shadows and lakes are similar. However, when exploring the pixel values of shadows and water bodies in the thermal band 6 (Landsat 5), values were much higher for water bodies than in shadows. Hence, a thresholding value of 105 (DN values) was applied on the summer imagery to remove shadows from the water mask (fig. 14d). Nevertheless, noisy pixels still remained and were deleted based on area; polygons below 2700 m^2 (equivalent of 3 Landsat pixels) were removed. Finally, processes that are not icing-related are sometimes responsible for substantial snow and ice accumulation along the shorelines of rivers and lakes past the snowmelt period. This remnant ice and snow was eliminated from the classification by growing the water mask outwards by 1,5 times the pixel dimension (45 m) (Morse and Wolfe, 2015).

Following these steps, each scene resulted in a binary raster; where 0 indicated "no ice" and 1 indicated icing. To calculate icing recurrence, a raster containing the total image count for a given Landsat extent was created and used to normalize the dataset across the study area as the number of scenes varied between Landsat extents (fig. 10). The *Editor Toolbar* was used to trace a polygon over each scene extent, where a field was added to every polygon created, specifying the scene count in the image stack. The polygons were converted to raster using the *Polygon to Raster* tool, where IMAGE_COUNT was specified as the value field. To obtain percentage of recurrence, binary rasters from a stack were added together using the *Raster Calculator* and then divided by the amount of scenes in that stack. For example, a recurrence of 70% would be explained by a given pixel observed as "iced" 7 times in a stack of 10 images.

Using the *Raster to Polygon* tool, icing polygons were created from the recurrence map; pixels with a value >30 (%) were selected (note, the option *Simplify Polygons* was not selected in order

to retain the pixel's edge). Polygon attributes such as coordinates (both UTM and decimal degrees) and surface area (in m^2) were calculated with the *Calculate Geometry* function. Then, the *Calculate Geometry* function permitted to obtain polygon centroids and to convert the latter into point features.

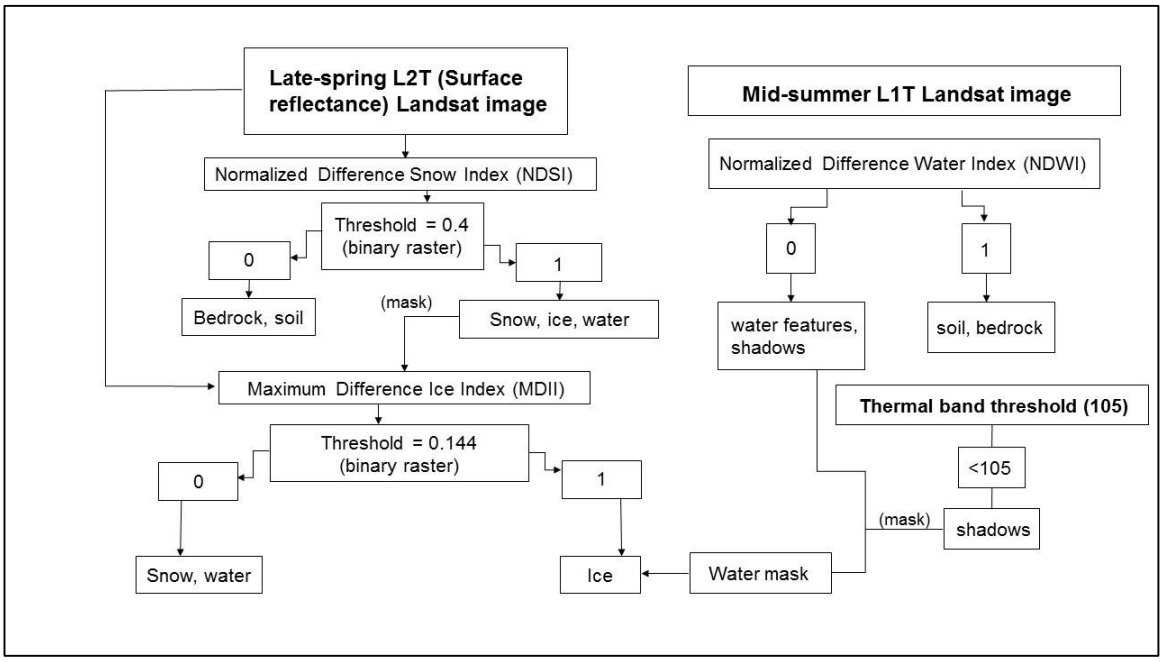

Figure 12. Flowchart of the image processing methodology.

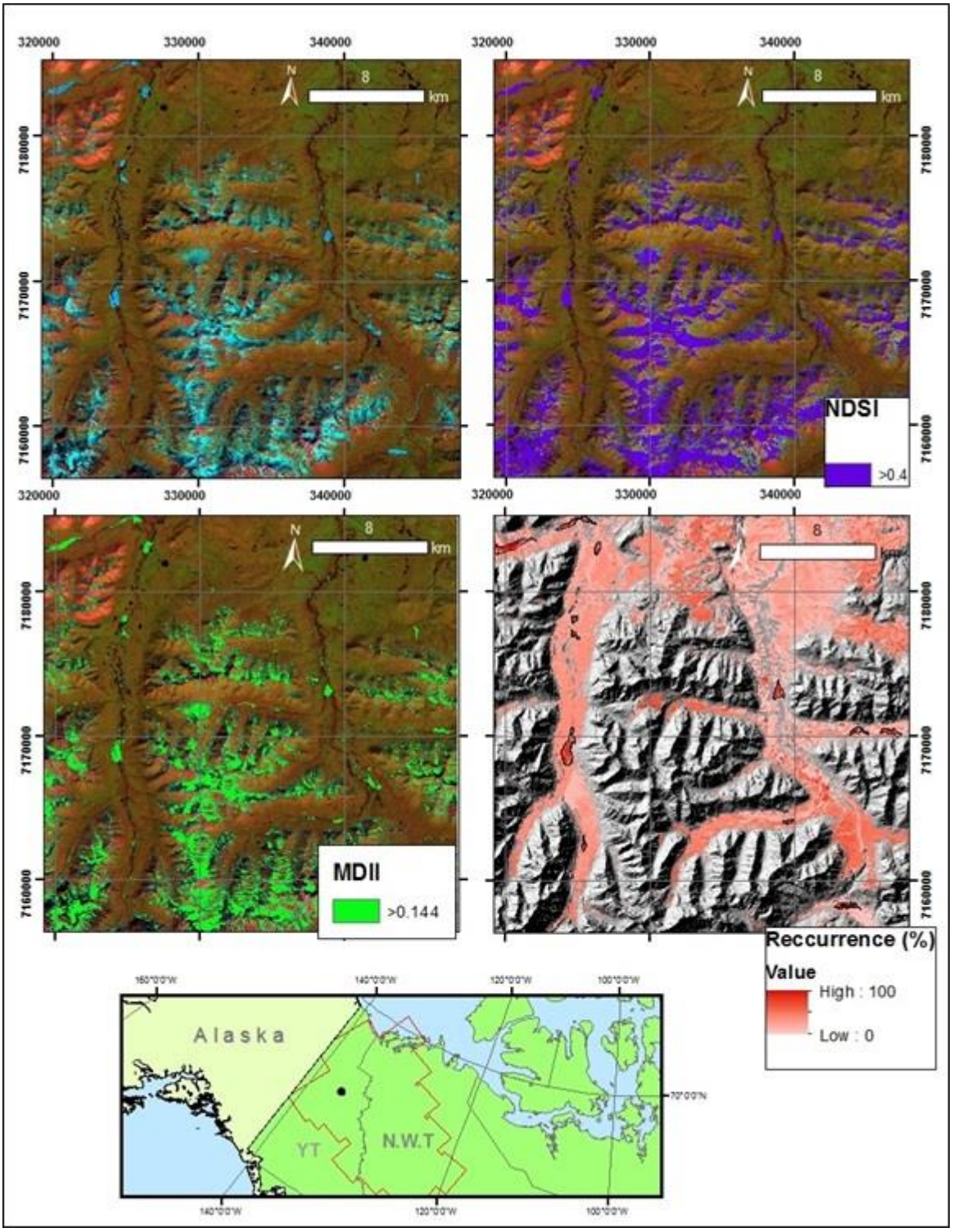

Figure 13. Montage demonstrating classification steps. Top left; Landsat 5 false-color composite (7,4,2). Top right; NDSI thresholded to >0,4. Bottom left; MDII performed within NDSI masked pixels, threshold at 0.144. Bottom right; recurrence raster with >30% pixels outlined in black.

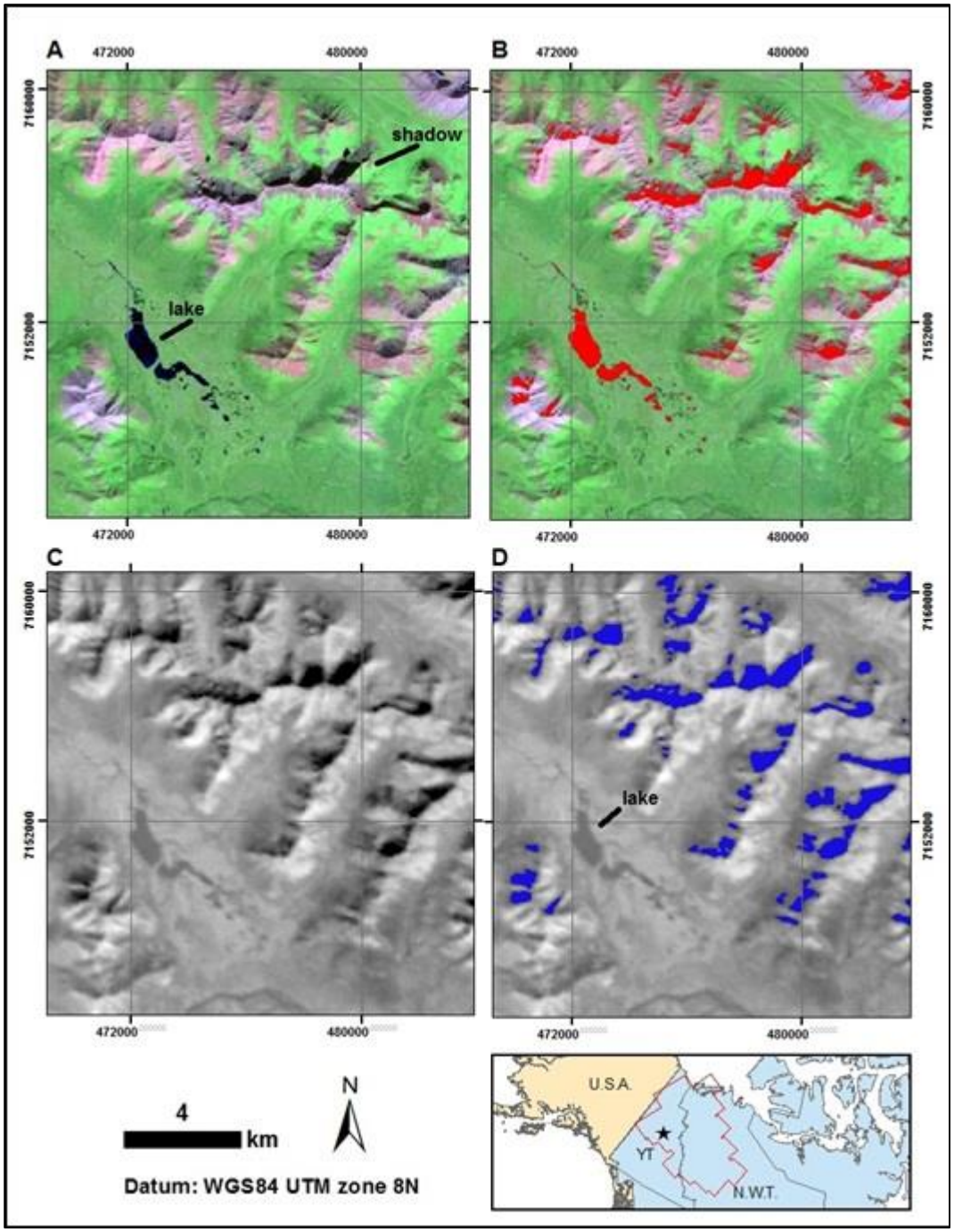

Figure 14. Montage showing masking steps using a thermal band threshold. A) Mid-summer Landsat 5 (LT05_L1TP2003080920) Natural-color composite. B) NDWI shown in red. C) Landsat 5 (LT05_L1TP2003080920) thermal band. D) Thermal band threshold (<105) showing shadowed areas without the inclusion of water bodies.

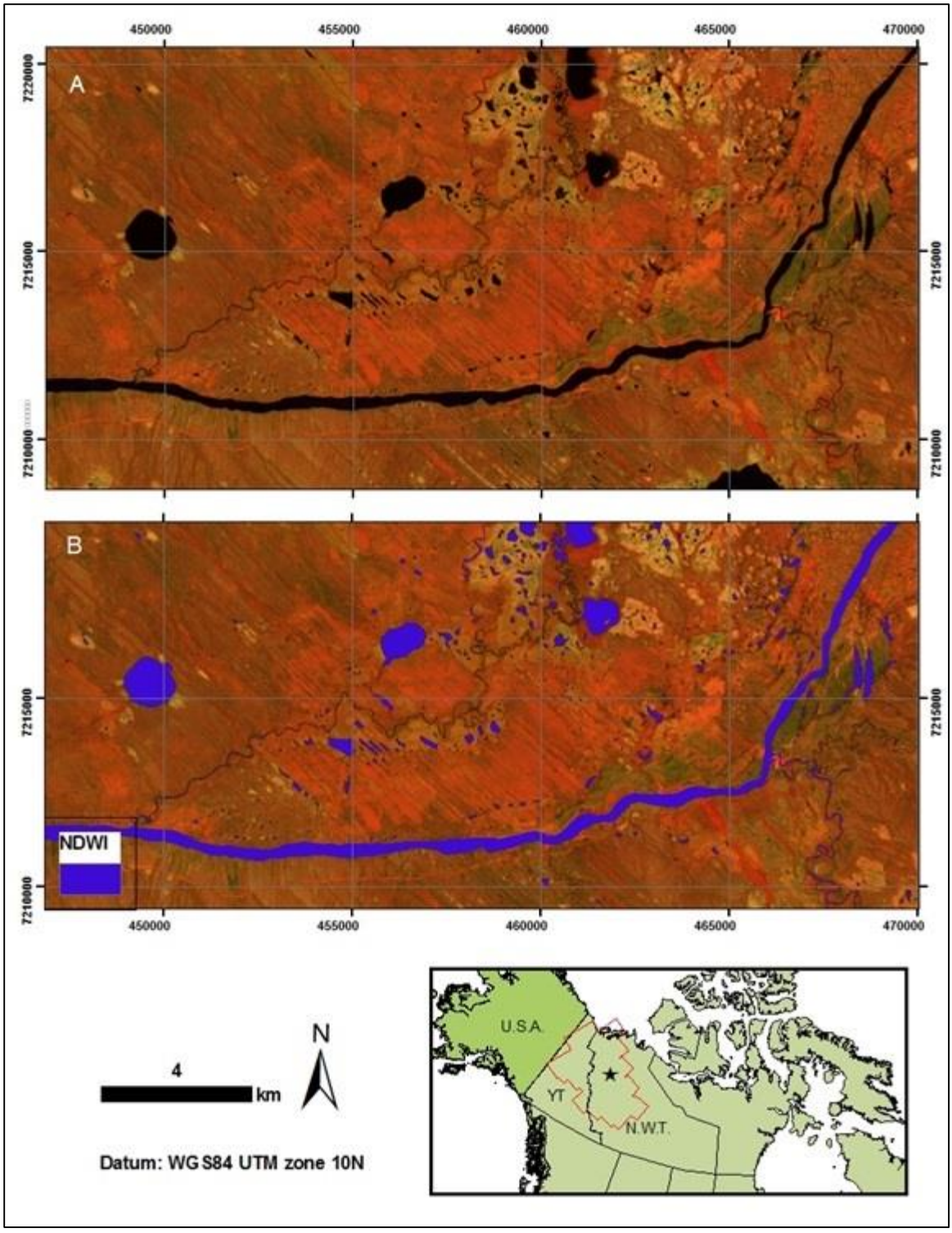

Figure 15. Montage showing NDWI masking where no shadows are created from topography A) Landsat 5 (LT05_L1TP05401419900610) false-color composite (7,4,2) of Great Bear River near Deline. B) NDWI result (shown in purple).

4.4 Spatial control on icing distribution

Relations between the spatial distribution of icings and terrain factors, drainage area, ecoregions, permafrost type, surface geology, bedrock geology and proximity to faults were investigated in ArcGIS using the centroid of each icing and the *Extract Multi Values to Points* tool. Terrain attributes, which include elevation, slope and aspect, were derived using ArcGIS (Spatial Analyst) using a mosaicked 30 m DEM from the Canadian Digital Elevation Model. The drainage area was derived from the the National Hydro Network *GeoBase Series* 1:50 000 scale watershed data. The CanBPv0 blended precipitation data from meteorological station data and satellite estimates (Lin and Wang, 2011) was used to calculate total amount of precipitation received in each watershed and its relation with extent of icings (https://open.canada.ca/data/en/dataset/5d49713a-fe56-48a8-887f-c0ca3e4aebfe). The distribution of permafrost in the study area was derived from the Geological Survey of Canada Bulletin 548 (Smith et *al.*, 2001). Digital data of surficial geology was acquired from the Canadian Geoscience Map 195. Geological faults and parent bedrock were derived from the Geological Survey of Yukon (http://www.geology.gov.yk.ca/) and Northwest Territories Geological Survey (https://datahub-ntgs.opendata.arcgis.com/) and merged to cover to the study area. The proximity of icings to faults was assessed using the *Near* tool that calculates shortest distance between each single icing point and the nearest fault.

4.5 Validation of approach

To validate the identification and extent of icings from the semi-automated approach, the results were compared to: 1) known location of icings in the study area (e.g. Lauriol et *al.*, 1991; Clark & Lauriol, 1997); and 2) late-winter high-resolution imagery from WorldView-2 and GeoEye-1 (0.46m and 0.41m multispectral resolution, respectively). Although the presence of substantial

snow cover throughout the river valley can conceal river ice, icings can be easily distinguished by its blueish color (Kane, 1981).

4.6 River discharge records

Considering that icings form during winter along fluvial channels that freeze to the bed, which confines baseflow and generates hydrostatic conditions for groundwater to seep to the surface, discharge records from 17 rivers with watershed extent <25,000 km^2 in the study area were analyzed for trends in total annual discharge and winter baseflow (Water Survey of Canada's Hydrometric Database; http://www.wsc.ec.gc.ca/). Excluding the gauging stations along major rivers (i.e., Mackenzie, Yukon rivers) because icings do not develop along them, the selected stations represent ~70% of the year-round active stations; the others had discontinuous records. Mean monthly discharge data was available for most years between 1970 and 2016 . All 17 rivers develop an ice cover during the winter such that baseflow is sustained by groundwater discharge. Total annual discharge and groundwater contribution during the winter months (December 1 to March 31) were converted to $m^3\ yr^{-1}$ of water flow. Analyses of long-term trends in total annual discharge and winter groundwater contribution were performed using the Mann-Kendall test, with linear changes represented with the Sen slope (i.e., Dery et al., 2005; Walvoord et al., 2007). Spectral analysis was performed on detrended annual winter discharge to identify significant cycles related to climate phenomena.

Results

5.1 Distribution of icings in northwestern Canada

In the study area, a total of 1402 icings with recurrence intervals > 30% were identified (figure 16). Known icing occurrences in Tombstone Territorial Park and in northern YT and adjacent NWT were identified in the mapping (i.e,. Lauriol et al., 1991). Additionally, a comparison with late-winter high-resolution imagery confirmed the presence of icings in the Sahtu highlands and on the Hare Indian river (figure 25 and 26, respectively). The average surface area of the icings was 0.2 km^2; out of all icings, 19 "mega icings" had surface areas above 2 km^2 (figure 16). These mega icings account for 21% of the total icing area in the region; the cumulative icing surface area is 277 km^2 and accounts for 0.04% of the total study area. Note, these "mega-icings" had not been mapped by previous research.

The highest icing count was found in the Mackenzie Mountains, which contained more than half of the total icings identified (718 icings). When the frequency of icing count is normalized by the frequency distribution of area covered by the ecoregions, the icings are more likely to occur in mountainous regions by factors of 2.9 to 1.3: the Mackenzie (factor of 2.9), followed by the North Ogilvie (2.0x), British-Richardson (1.4x) and Selwynn Mountains (1.3x); the lowlands contained the lowest likelihood of icing distribution (< 0.3x). Icings were found at elevations ranging between 15 and 2022 m a.s.l. (figure 17b). Normalizing the frequency count of icings by the frequency distribution of elevation in the study area reveals that icings are more likely to occur at elevations of 500-1300 m by factors of 1.2 to 3.8. In terms of type of surficial geology, icings are more likely to occur by factors of 1.2 to 4.2 on undifferentiated bedrock, colluvial mass-wasting deposits (both veneer and undifferentiated) and veneers of glacial sediments (figure 17f). The majority of icings are found in carbonate, sandstone and evaporite rocks; few

are found in volcanic rocks. The majority of icings (84%) were within 6 km from the nearest geological fault: average distance being 5 km and only 25 icings were found at distances of 20-207 km (figure 17d). Most of the icings (n=1174) were found in the continuous permafrost zone. Normalized to the frequency distribution of permafrost zones, icings are more likely to occur in continuous permafrost by a factor of 1.5; the others occurred in the zone of extensive discontinuous permafrost.

Table 4. Area and latitude and longitude in decimal degrees of the 19 "mega icings".

River	area km2	x_dd	y_dd
North Nahanni	7.70	-125.62	62.43
Ogilvie (tributary)	5.21	-139.06	64.95
North Nahanni	4.37	-124.72	62.33
South McQuesten (tributary)	4.32	-135.31	64.12
Babagge	3.89	-139.27	68.65
Babagge	3.19	-139.16	68.68
Root	3.15	-125.50	62.97
Root	2.94	-125.32	62.97
Wind	2.71	-134.60	64.71
Little Keele	2.55	-127.43	64.71
Silverberry	2.39	-126.43	62.91
Wind	2.30	-134.78	64.98
South McQuesten (tributary)	2.26	-135.36	64.09
Wind	2.23	-135.16	65.15
Root	2.22	-125.57	62.93
Carcajou	2.21	-127.92	64.46
English Chief	2.11	-124.54	62.58
Wind (tributary)	2.09	-134.33	64.83
Carcajou	2.08	-127.83	64.49

5.2 Icing distribution in relation to watersheds

Icings occurred in 19 of the 55 watersheds in the study area. In the study area, icings are all found in watersheds with extents < 26,200 km^2 in the discontinuous permafrost and < 35,800 km^2 in continuous permafrost. When normalized by the frequency distribution of area covered by

the watersheds, icings are more likely to occur in the upper Porcupine, Root, Carcajou, Ontaratue and Redstone watersheds by factors of 6.5 to 1.1 (figure 17g). These five watersheds represent 29% of the study area and contain 78% of the icings. The larger icings in the study area were observed on the North Nahanni river (7.7 km^2), on a tributary of the Ogilvie river (5.2 km^2) and on the Babbage river (3.8 km^2); however, the largest icing in in northwestern Canada is the upper Firth river icing (~31 km^2) (Clark and Lauriol, 1997). The number of icings and their mean surface area showed no relation with watershed extent in which they occur (figure 18). However, the maximum and cumulative surface area of icings were positively correlated with their watershed extent, with relations being significant in the continuous permafrost zone (figure 19d). Considering that the groundwater feeding the icings is recharged from precipitation received within the watershed, the relation with total precipitation in the watershed and icings was explored. Here, the maximum and cumulative surface area of icings revealed significant positive relation with total precipitation in continuous permafrost catchments (figure 19). Although the thickness of the individual icings was not determined, it generally varies between 2-3 m (Lauriol et *al.,* 1991; Clark and Lauriol, 1997). Using an ice thickness of 2 m, an average of 0.33 ± 0.28% of total annual precipitation within the watersheds is stored in icings, and it increases to 0.51 ± 0.44% if a thickness of 3 m is used.

5.3 River discharge in northwestern Canada

Out of the 17 gauging stations, 13 are situated in watersheds that contain icings and 8 of them are along a river with at least one icing. The total annual discharge of the 17 rivers range from 6.2 $10^{\wedge 7}$ to 6.1 $10^{\wedge 9}$ m^3 yr^{-1} and is significantly correlated with watershed extent (figure 22a). The winter discharge range from 8.4 $10^{\wedge 4}$ to 8.3 $10^{\wedge 8}$ m^3 yr^{-1} and is also significantly correlated with watershed extent (figure 22b). However, despite having similar regression slope values, the

rivers in continuous permafrost have much lower intercept value, meaning that for similar watershed extents, the winter discharge in continuous permafrost is about one order of magnitude lower than in the discontinuous permafrost zone.

Estimates of average winter groundwater contribution to total annual discharge at the 17 gauging stations over the individual periods of record ranged from 0.1 to 22% (Table 5). The Babbage, Rat and Eagle rivers had the lowest winter contribution (<2%), whereas the Beaver, North Klondike and Caribou rivers had the highest (20-22%). However, the average winter groundwater contribution to total annual discharge showed distinct trends with respect to permafrost zone. Rivers located in the discontinuous permafrost zone had the highest winter contribution (14-22%) but showed a significant negative trend with watershed extent (figure 22c). By contrast, the average winter groundwater contribution to rivers located in the continuous permafrost zone ranged from 0.1 to 14.1% and showed a significant positive trend with watershed extent (figure 22c).

Most discharge records showed an increase in winter groundwater contribution to the total annual discharge over the 1970-2016 period (figure 22d). Out of the 17 rivers, 7 of them revealed a significant increase in winter contribution; only the Whitestone and Redstone rivers showed a non-significant decreasing trend. In regards to total annual discharge, only the Root River and Caribou Creek showed a significant increase in total annual discharge; 12 rivers showed a non-significant increasing trend; the other 3 rivers showed a non-significant decreasing trend (Fig. 20). In general, change in winter contributions were positively correlated with changes in total annual discharge.

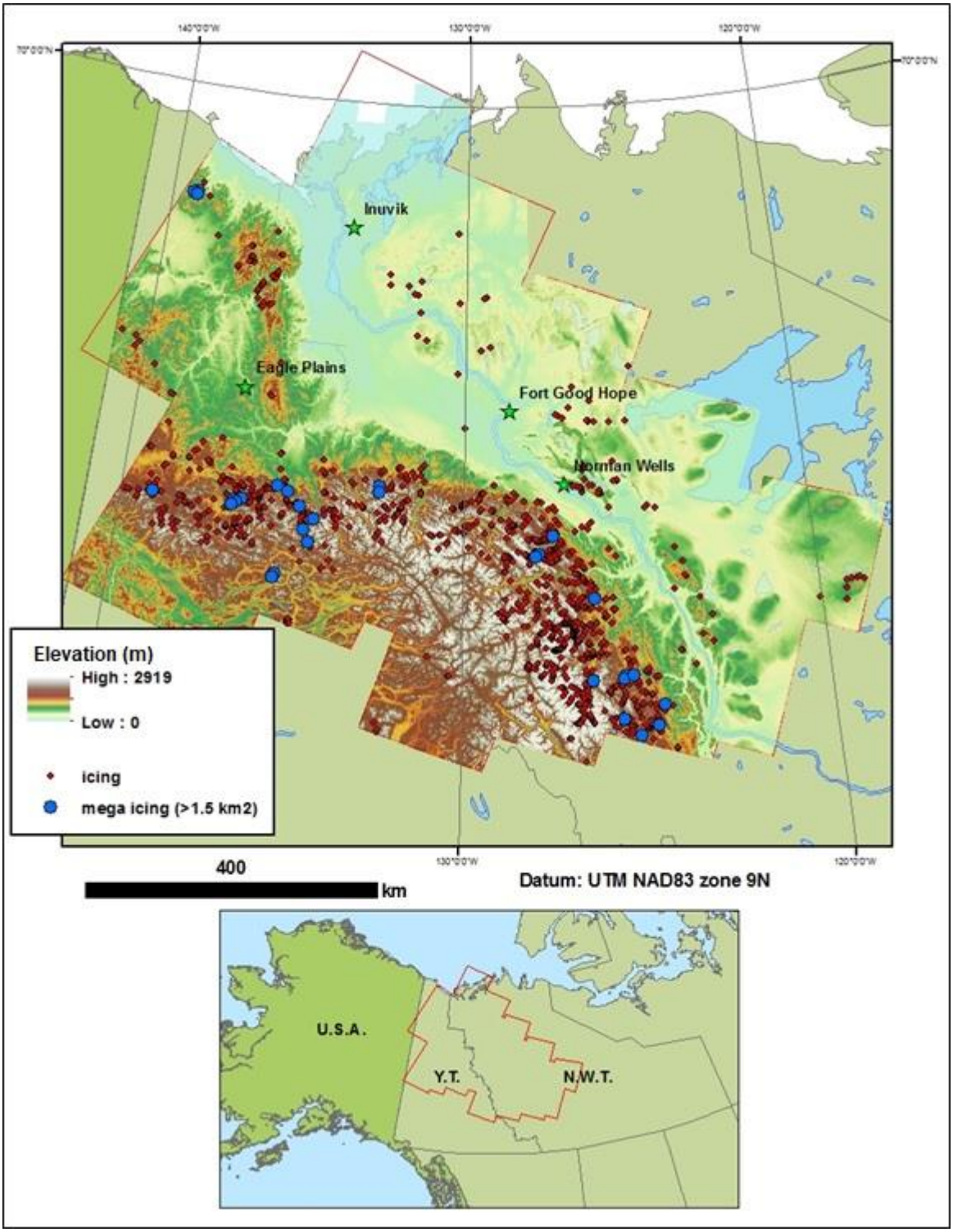

Figure 16. Map of icing occurrence.

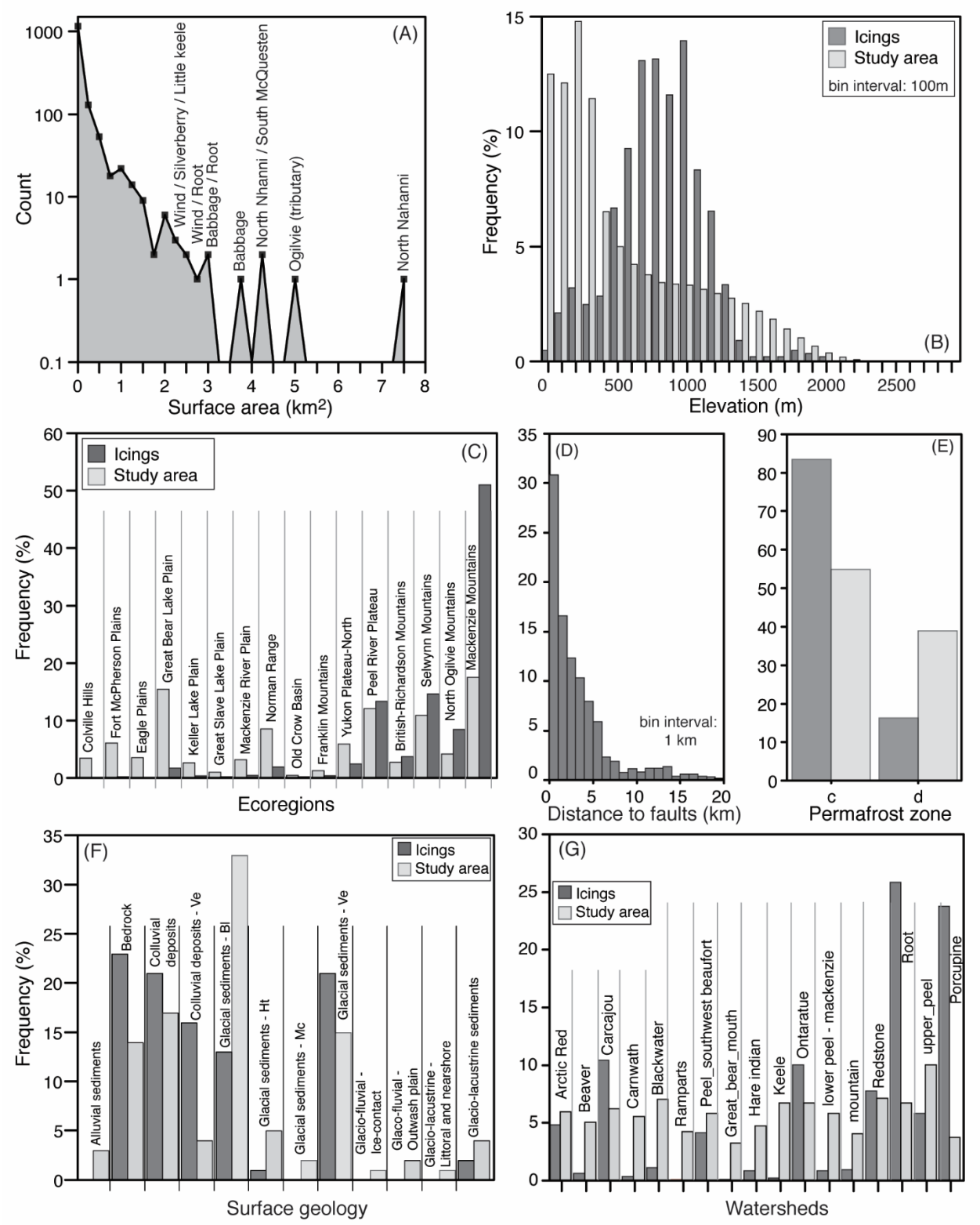

Figure 17. A) Frequency distribution of icing surface area. B) Frequency distribution of icing and study area elevation. C) Frequency distribution of icings and ecoregions D) Frequency distribution of icing distance to the nearest geological fault. E) Icing frequency distribution by underlying permafrost type. F) Frequency of icings and surface area of surficial geology. G) Frequency of icings and surface area of watersheds found in the study area.

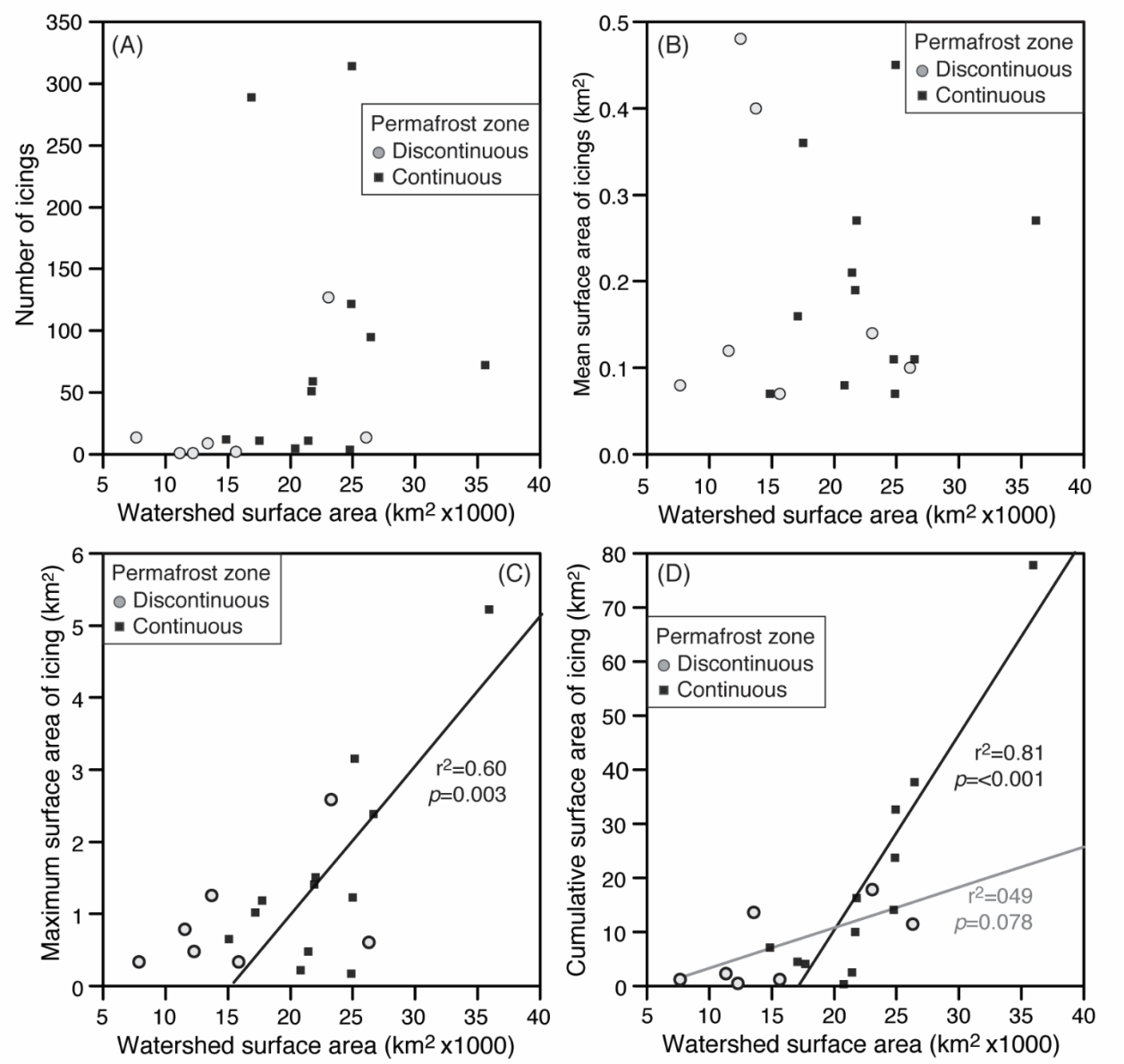

Figure 18. Plot of watershed surface area relative to A) icing frequency B) mean surface area of icings C) maximum icing surface area D) cumulative icing surface area.

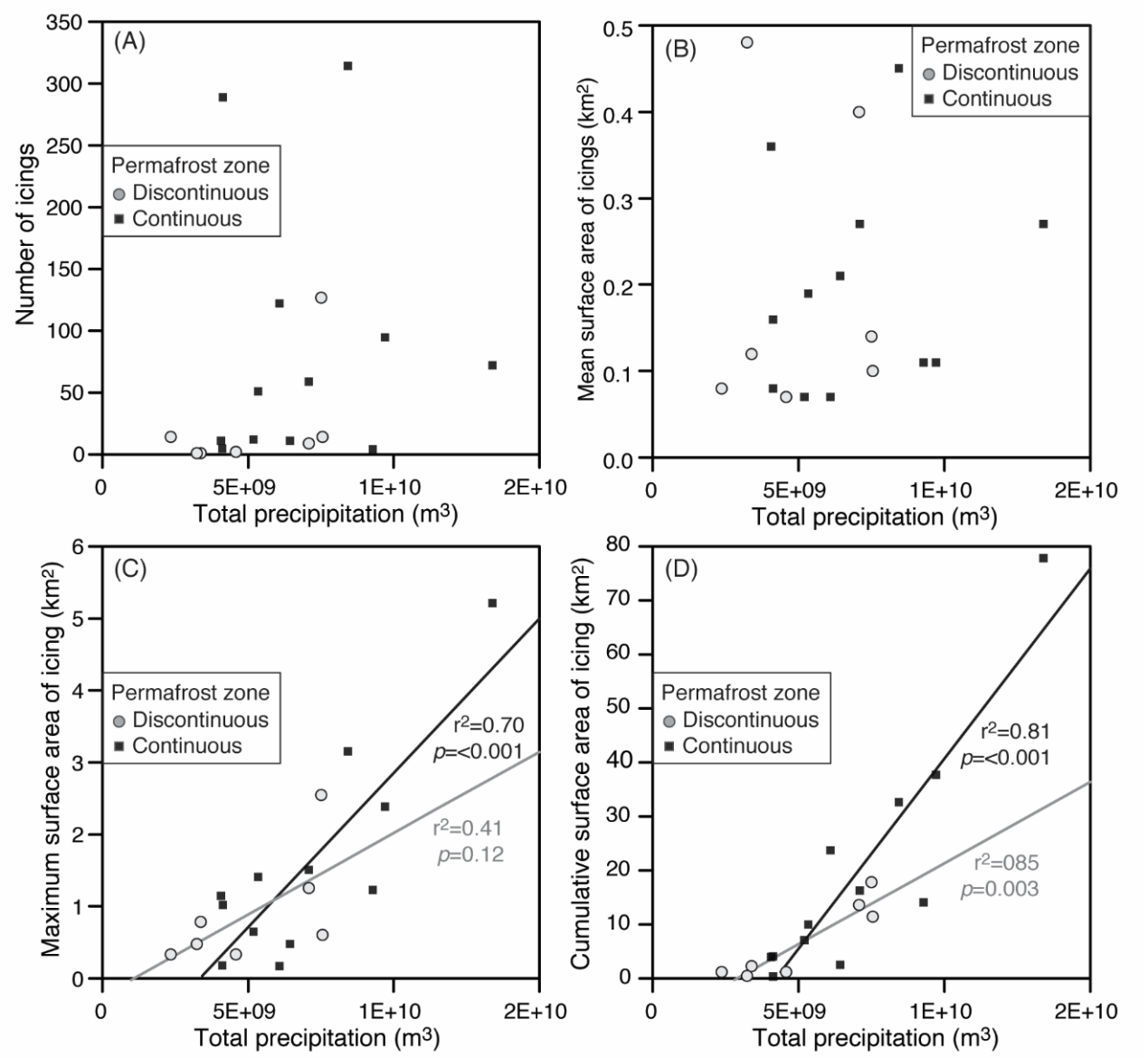

Figure 19. Plot of total precipitation per watershed relative to A) icing frequency B) mean icing surface area C) maximum icing surface area D) cumulative icing surface area.

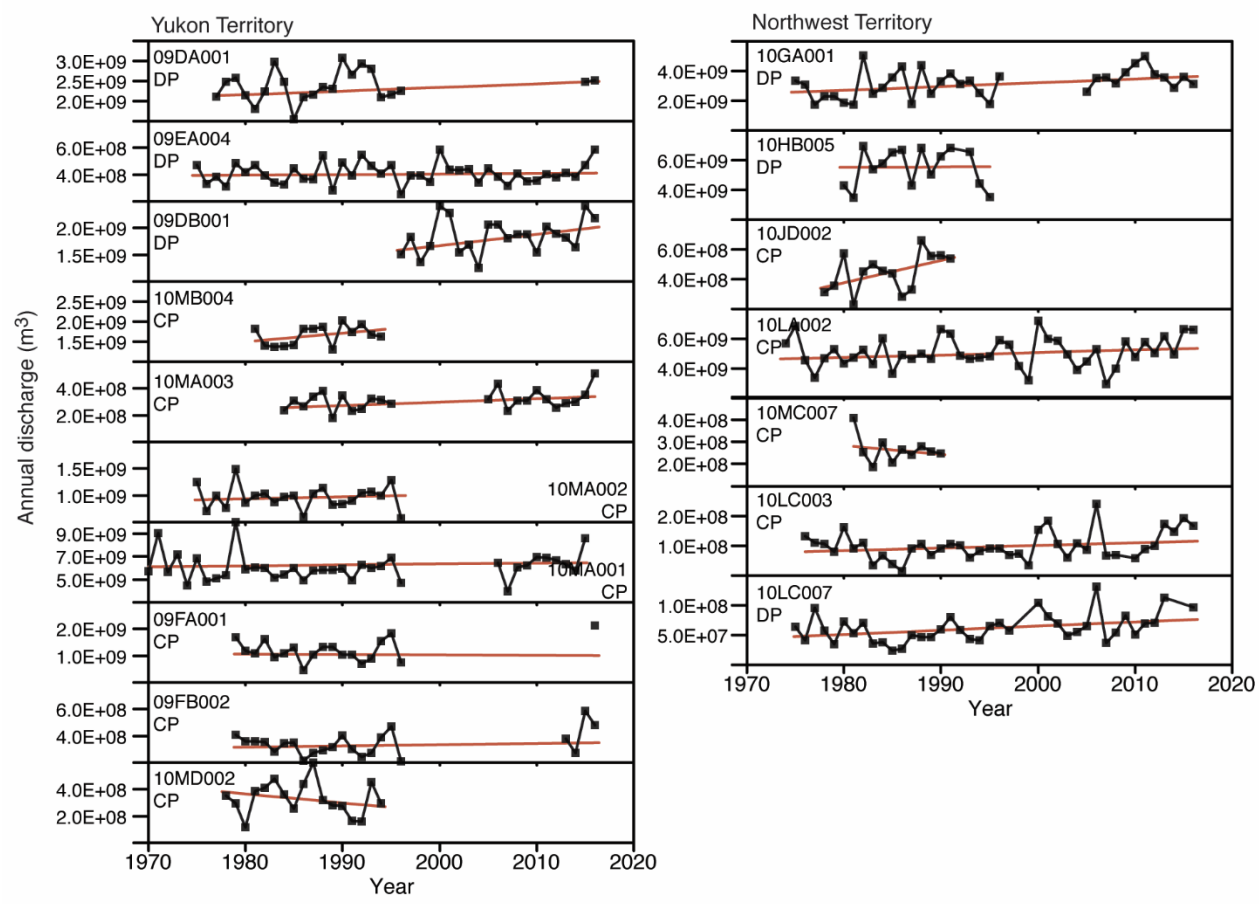

Figure 20. Montage showing signal processing of annual river discharge from different gauge stations located in the study area.

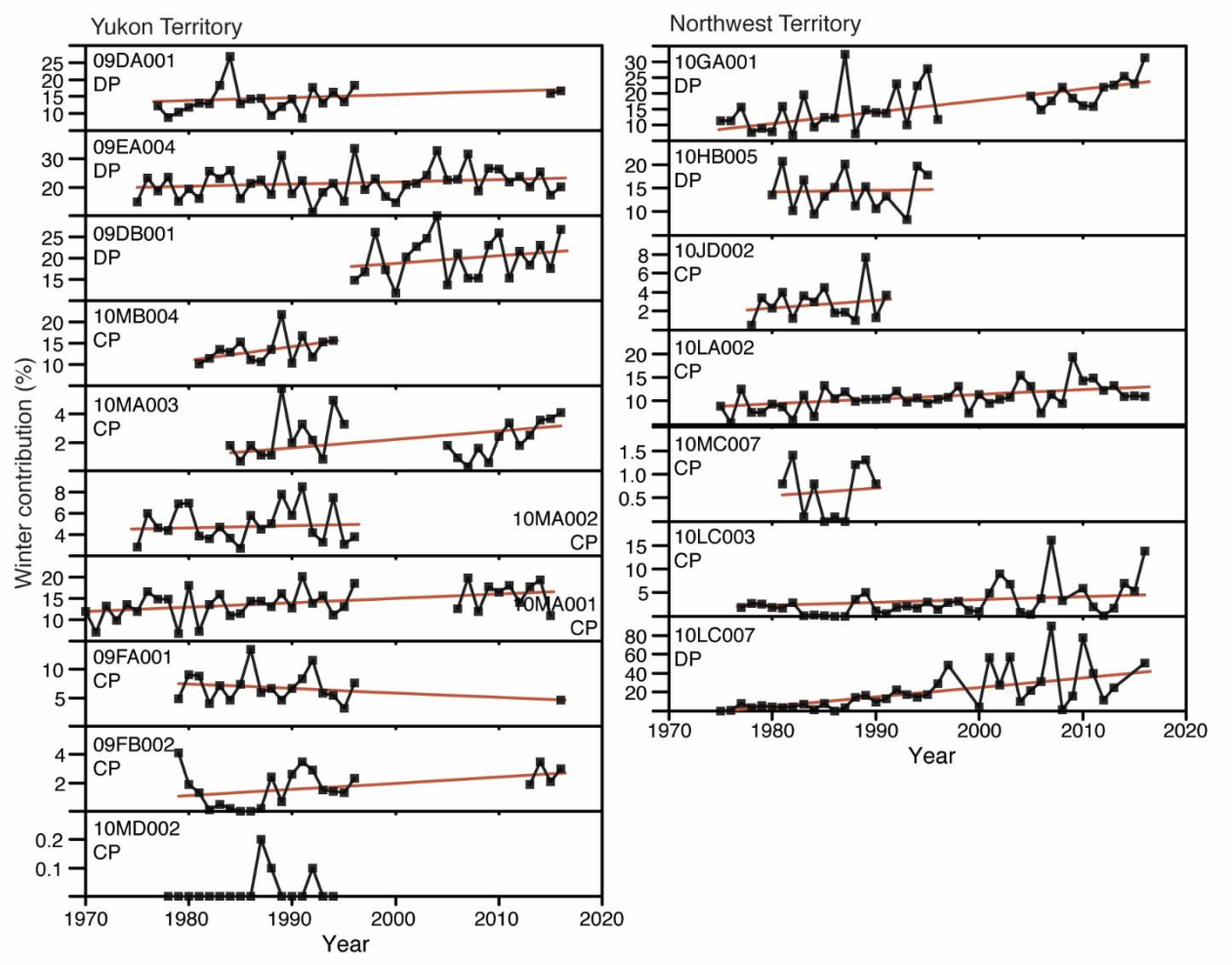

Figure 21. Montage showing signal processing of winter contribution to total annual discharge from different gauge stations located in the study area.

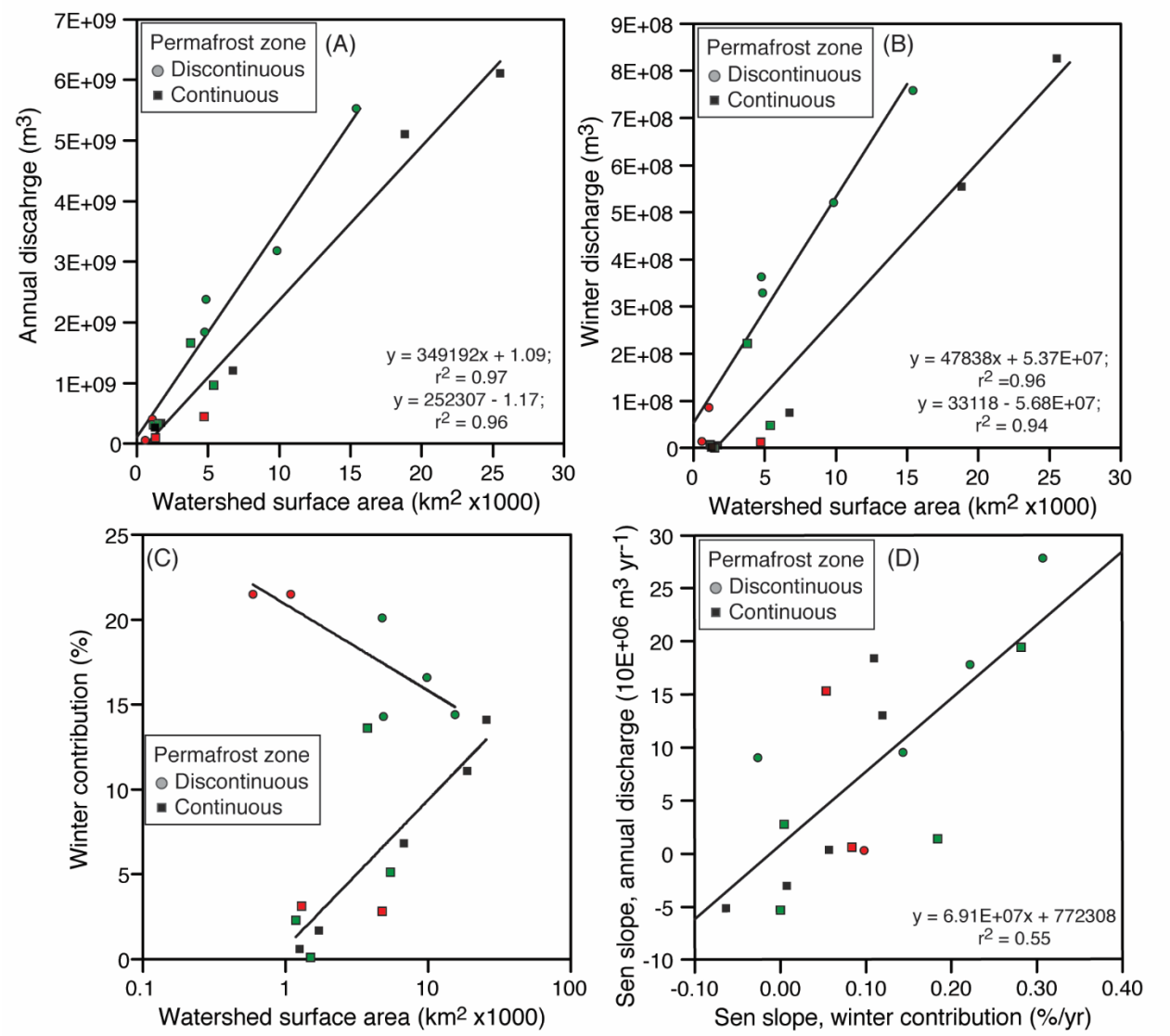

Figure 22. (A) Annual drainage gauge data plotted against drainage area. (B) Baseflow discharge (winter discharge) plotted against drainage area. (C) Winter contribution (%) plotted against drainage area. (D) Variation in annual discharge plotted against change in winter contribution.

Table 5. Hydrometric data from gauging stations spread across the study area.

Station ID	Station name	First year	Last year	Drainage area (km2)		Annual (km3/yr)	Winter %	Winter (%/yr)		permafrost
09DA001	HESS RIVER ABOVE EMERALD CREEK	*1977*	*2016*	4840	2.38E+09	9.49E+06	14.3	0.144	+	D
09DB001	BEAVER RIVER BELOW MATSON CREEK	*1996*	*2016*	4770	1.85E+09	1.78E+07	20.1	0.222		D
09EA004	NORTH KLONDIKE RIVER NEAR THE MOUTH	*1975*	*2016*	1090	4.11E+08	3.08E+05	21.5	0.098		D
09FA001	WHITESTONE RIVER NEAR THE MOUTH	*1979*	*2016*	6730	1.21E+09	-5.16E+06	6.8	-0.063		C
09FB002	EAGLE RIVER AT DEMPSTER HIGHWAY BRIDGE	*1945*	*2016*	1720	3.44E+08	3.46E+05	1.7	0.057	+	C
10MA001	PEEL RIVER ABOVE CANYON CREEK	*1970*	*2016*	25500	6.11E+09	1.84E+07	14.1	**0.110**	*	C
10MA002	OGILVIE RIVER AT KILOMETRE 197.9 DEMPSTER HIGHWAY	*1975*	*1996*	5410	9.66E+08	2.73E+06	5.1	0.005		C
10MA003	BLACKSTONE RIVER NEAR CHAPMAN LAKE AIRSTRIP	*1984*	*1995*	1180	3.12E+08	1.35E+06	2.3	0.184		C
10MB004	BONNET PLUME RIVER ABOVE GILLESPIE CREEK	*1981*	*1994*	3760	1.66E+09	1.94E+07	13.6	0.282		C
10MD002	BABBAGE RIVER BELOW CARIBOU CREEK	*1978*	*1994*	1500	3.32E+08	-5.34E+06	0.1	0.000		C
10ED002	LIARD RIVER NEAR THE MOUTH	*1973*	*2016*	275000	7.93E+10	1.43E+08	21.9	**0.151**	**	D
10GA001	ROOT RIVER NEAR THE MOUTH	*1975*	*2016*	9820	3.18E+09	**2.78E+07**	16.6	**0.307**	***	D
10HB005	REDSTONE RIVER 63 KM ABOVE THE MOUTH	*1980*	*1995*	15400	5.53E+09	9.01E+06	14.4	-0.026		D
10JD002	WHITEFISH RIVER NEAR THE MOUTH	*1978*	*1991*	4740	4.47E+08	1.53E+07	2.8	0.054		C
10LA002	ARCTIC RED RIVER NEAR THE MOUTH	*1974*	*2016*	18800	5.11E+09	1.30E+07	11.1	**0.120**	***	C
10LC003	RENGLENG RIVER BELOW HIGHWAY NO. 8	*1976*	*2016*	1300	1.01E+08	6.11E+05	3.1	**0.084**	**	C/D
10LC007	CARIBOU CREEK ABOVE HIGHWAY NO. 8	*1975*	*2016*	590	62253920	**7.23E+05**	21.5	**0.974**	***	C/D
10MC002	PEEL RIVER ABOVE FORT MCPHERSO	*1975*	*2016*	70600	2.19E+10	1.71E+07	15.4	**0.155**	***	C
10MC007	RAT RIVER NEAR FORT MCPHERSON	*1981*	*1990*	1260	2.64E+08	-3.01E+06	0.6	0.008		C

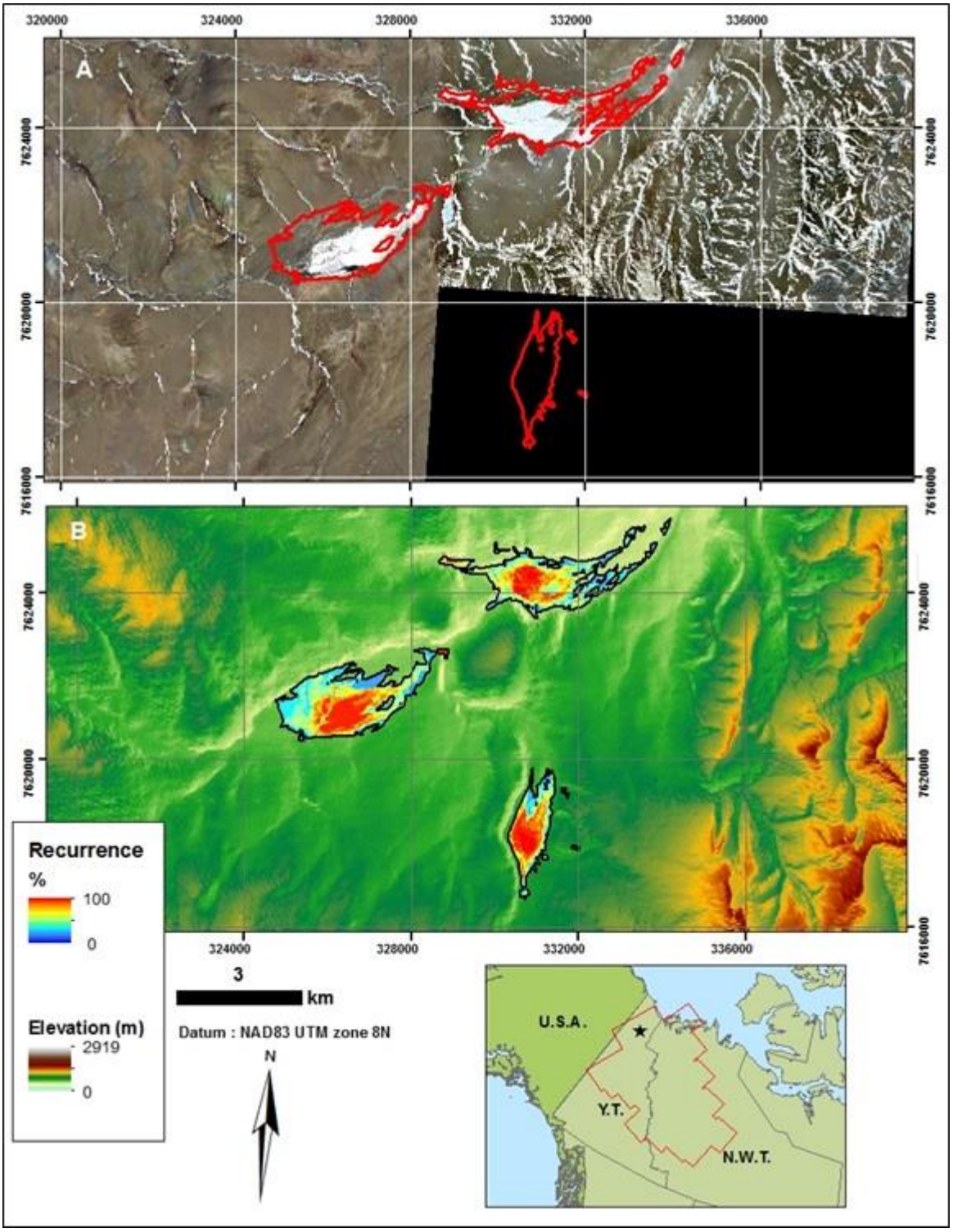

Figure 23. Montage showing A) WorldView-2 late-winter natural-composite image (May 24, 2012) with icing outline in red on the Babagge River, YT. B) Icing recurrence from classification on shaded-relief CDEM.

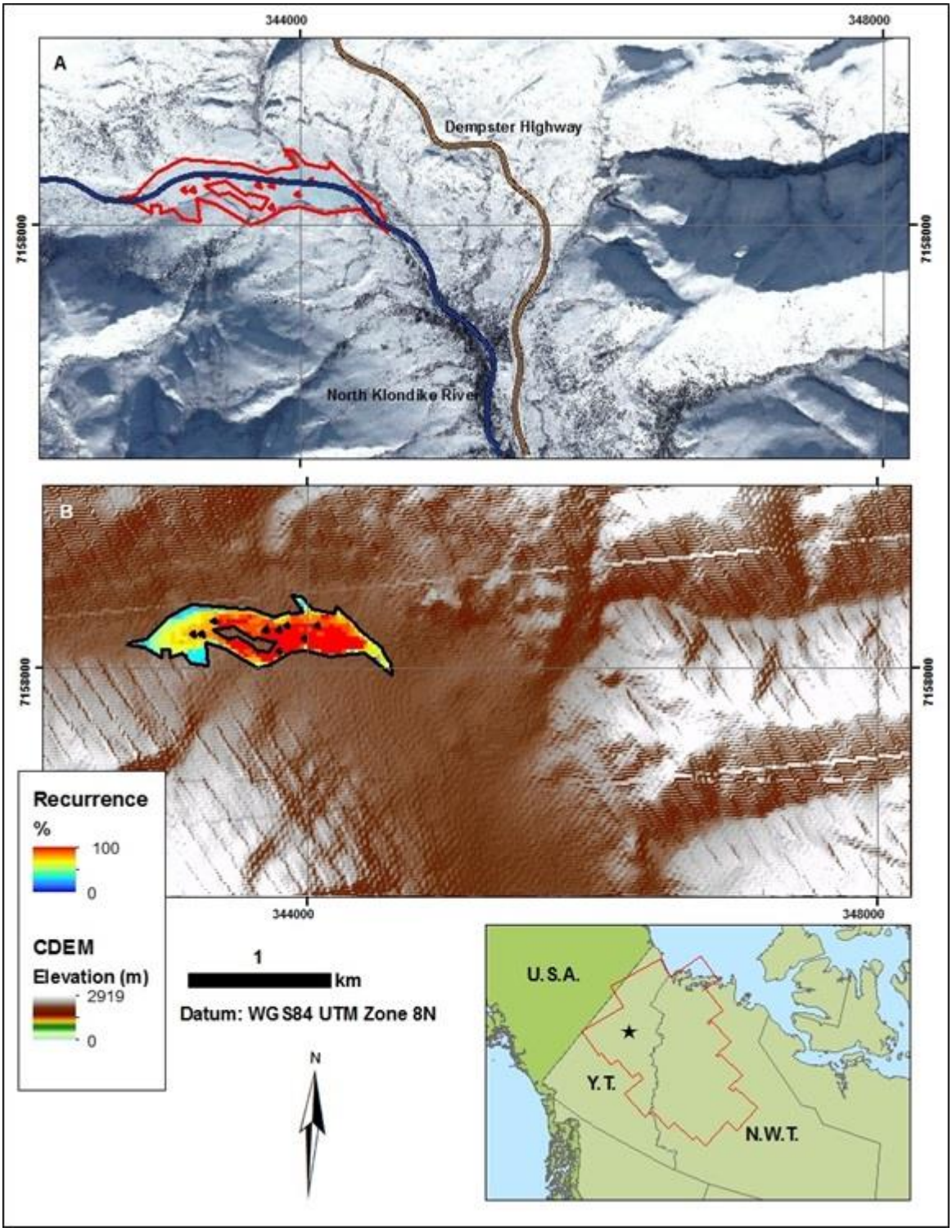

Figure 24. Montage showing A) WorldView-2 late-winter natural-composite image (March 14, 2014) with icing outline in red on the North Klondike River, YT. B) Icing recurrence from classification on shaded-relief CDEM.

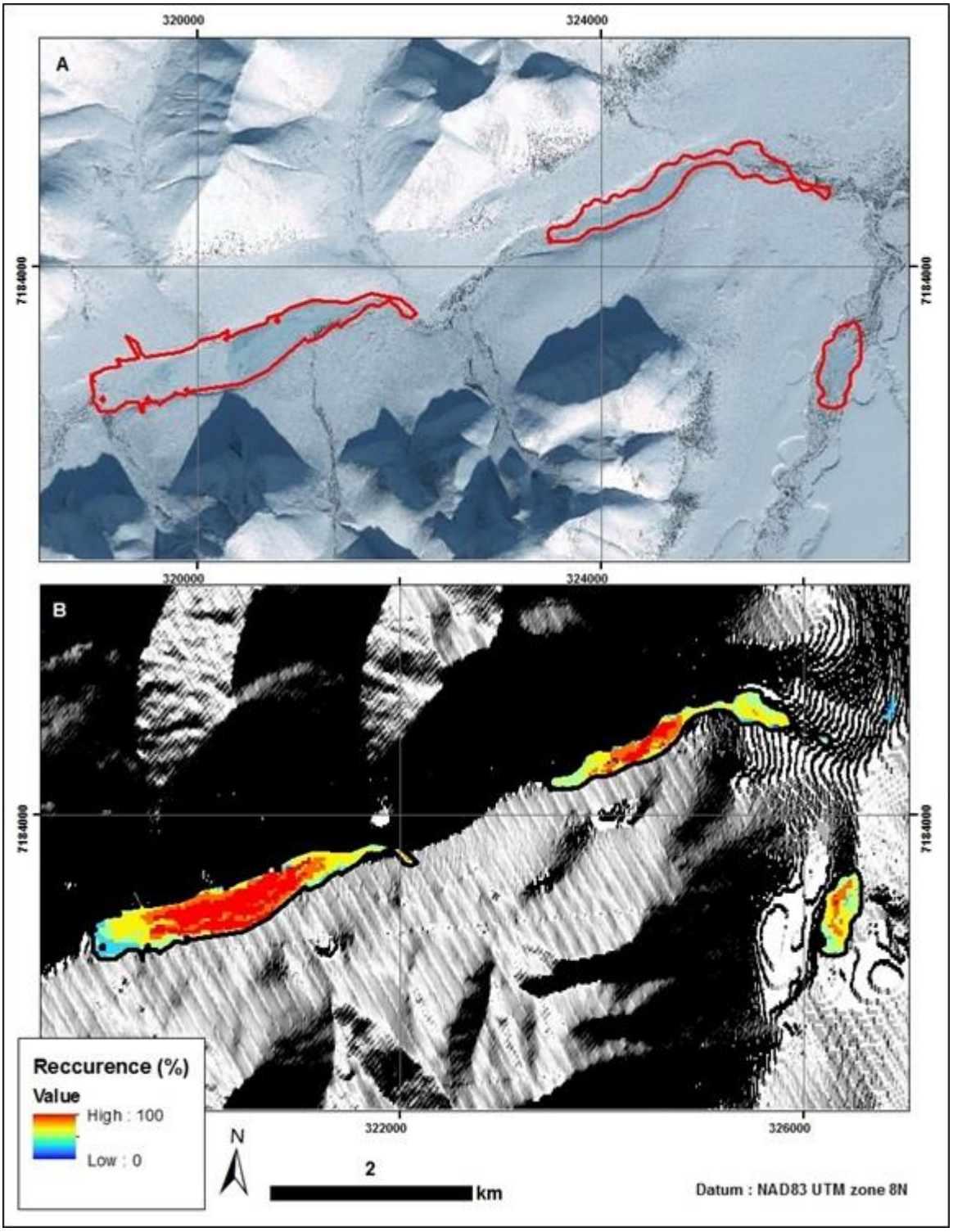

Figure 25. Montage showing A) WorldView-2 late-winter natural composite image (April 4th 2017) with icing outline in red on the Blackstone River, YT.. B) Icing outline with recurrence from classification on shaded-relief CDEM.

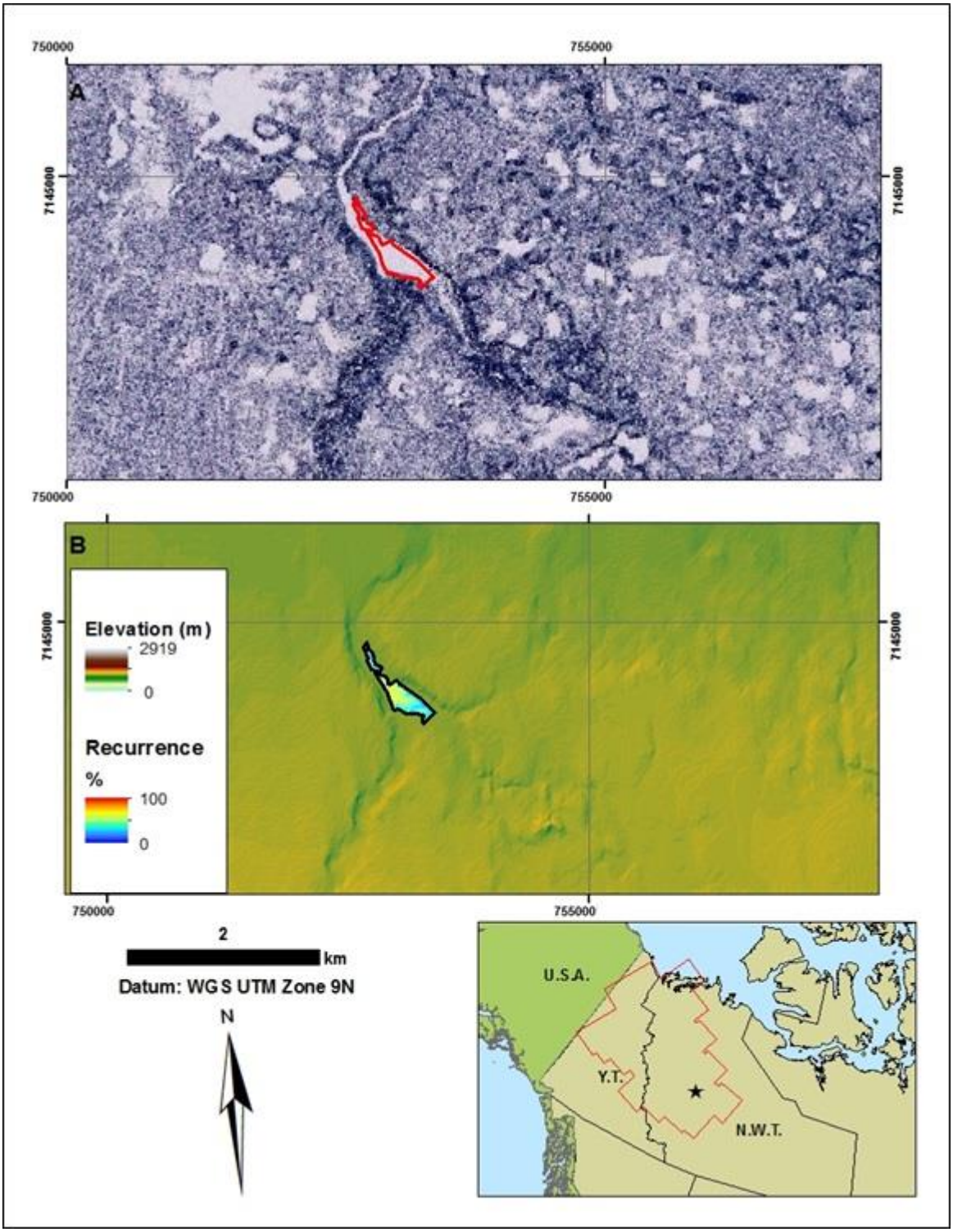

Figure 26. Montage showing A) Worldview-2 late-winter natural composite image (March 18th, 2017) with icing outline in red on southern limit of the Norman Range, N.W.T. B) Icing outiline with recurrence from classification on shaded-relief CDEM.

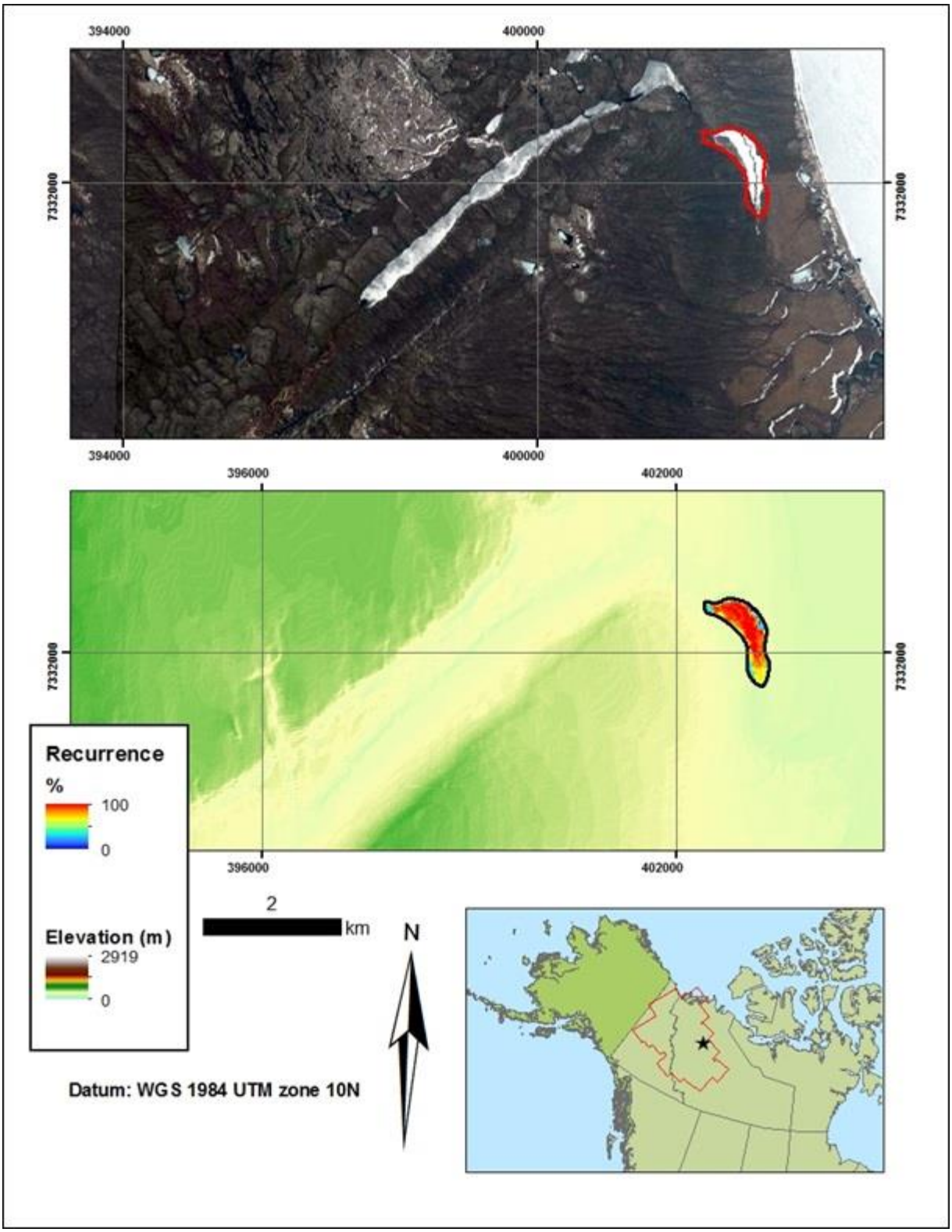

Figure 27. Montage showing A) Worldview-2 late-winter natural composite image (May 29th, 2018) with icing outline in red, west of the Great Slave Lake on the Hare Indian River, N.W.T. B) Icing outline with recurrence from classification on shaded-relief CDEM.

6. Discussion

Icings in the study area are most found at the foothills of karstic mountainous regions in the continuous permafrost zone (figure 16). Although the absence of a detailed investigation does not allow to confirm that each of the icings was associated with a groundwater spring, the late winter high-resolution satellite imageries show that the 5 rivers have a perennial spring that starts just upstream of the icings (e.g. figure 24).The icings also occur nearby fault zones which allows for groundwater discharge during the winter season (Michel, 1986; Lauriol et al. 1991; Kane et al., 2013). Wanty et *al.* (2010) found a similar relation between major fractures systems and distribution of icings in stream bottoms of the Shawnee Peak massif along the Alaska-Yukon border. In this region, the Occidental Creek valley had one the most extensive laterally fractured zone and contained the most extensive icing formation, both in terms of extent and thickness.

Insights into relations between groundwater flow and permafrost conditions can be gained from the occurrence of icings within the watersheds in the different permafrost zones. In the continuous permafrost zone, the cumulative surface area of icings, winter discharge and winter contribution to total annual discharge had significant positive relations with watershed extents (figure 22); a similar relation between cumulative surface area of icings and watershed extents in northern Yukon and northeast Alaska was also observed (Harden et al., 1977; Lauriol et al., 1991; McNamara et al., 1998). This suggest that groundwater flow through taliks in the karstic continuous permafrost is effective to transport water from recharge to source. In the case of river icings, the river must freeze to its bed in order to generate the hydrostatic pressure to force the groundwater to surface where it would freeze over the river ice, as such the location of icings along a river is determined by channel morphology (Kane 1981). The lower abundance of icings

in the discontinuous permafrost zone cannot be explained by the absence of perennial springs or winter air temperature being too warm. In fact, many springs have been identified in the discontinuous permafrost zone (Michel et al., 1986; Pollard and French, 1984). Additionnally, the number of freezing-days ranges from about 3700 in the discontinuous permafrost to about 4500 in the northern region (Smith et al., 2016b). However, the rivers in the discontinuous permafrost zone have higher winter discharge and winter contribution to total annual discharge relative to those in the continuous permafrost (figure 22). It is thus possible that the winter flow is too high and prevents freezing of the river to its bed. This was observed along the Fishing Branch by the inhabitants of Old Crow (Lauriol et al., 1991). An estimate of the winter flow conditions that support the development of river icings can be made from the occurrences of icings and winter discharge in their respective watersheds. Our results show that icings are generally found in watersheds with: 1) winter flow of 1-8 $10^{\wedge 8}$ m^3 (the four watersheds with gauging stations that do not contain icings have winter discharge < 1 $10^{\wedge 8}$ m^3); and 2) winter contribution to total annual discharge <20% (those with winter contribution > 20% do not have icings). Although these differences are based on the distribution of available gauging stations, it does seem to support the observation that the growth of icings require winter flow to be high enough to prevent complete freezing of the river but not too high to prevent freezing. Under these circumstances, icings would be sensitive to changing winter discharge conditions.

6.1 Fate of icings and changing groundwater and permafrost conditions

Walvoord and Striegl (2007) and St-Jacques & Sauchyn (2009) suggested that permafrost degradation might lead to increased groundwater contribution to total annual discharge in river systems. In northwestern Canada, winter discharge has shown to increase for most rivers in the study area since the 1970s (figure 21). Walvoord et al. (2012) forecasted baseflow and groundwater discharge in the Yukon Flats Basin, an area underlain by both continuous and discontinuous permafrost. Based on the projected warming trends, their simulations revealed that winter contribution and flow would increase substantially with decreasing permafrost coverage. The measured increase in groundwater discharge to rivers was consistent with historical trends in base flow observations in the Yukon River Basin and increased spatial extent of groundwater discharge in lowlands. Increased sub-surface drainage was caused by deeper flow paths of supra-permafrost water, expansion of taliks and also by increasing hydraulic conductivity of the icy permafrost soils as they approach 0C (e.g., Burt and Williams, 1976; Bense et al., 2009). However, changing groundwater flow was non-linear and most increase is predicted as permafrost extent decreases from 100% to ~70% (Walvoord et al., 2012). Along the boundary of discontinuous and continuous permafrost, the mean annual ground temperature is in the –2 to 0°C range, thus the hydraulic conductivity of the icy soils can rapidly increase as the ground temperature approaches 0^{o}C and allow for increased groundwater discharge. As such, the icings situated along the boundary of continuous permafrost are the most sensitive to degrading permafrost and the predicted increase in groundwater discharge. In northwestern Canada, 84 icings (6%) in the continuous permafrost zone are found with 10 km of that boundary and 564 icings (40%) are within 50 km.

7. Conclusion

To conclude, this research was able to create the most extensive map of icing occurrences of Mackenzie Valley Corridor and adjacent Yukon. This was done by adapting a method from Morse and Wolfe (2015) and by creating a new masking technique using Landsat's thermal band. Overall, this thesis had 3 objectives; 1) map the distribution of icings in the study area; 2) determine changes in winter baseflow conditions in watersheds of northwestern Canada; and 3) explore relations between the distribution of icings with terrain factors and winter groundwater conditions. Based on the results obtained, the following conclusions can be reached; i) icings tend to develop on terrain with slopes below 5^{o} and form in close proximity to geological faults; ii) undifferentiated bedrock, colluvial mass-wasting deposits and veneers of glacial sediments are common types of surficial geology where icings develop; iii) icings were mostly observed at the foothills of karstic mountainous regions and in continuous permafrost; iv) both precipitation volumes and watershed surface area show a strong relation with the cumulative icing surface area.

Based on the predicted climatic warming and increased precipitation in subarctic Canada, it can be expected that icings may develop later and degrade earlier, become thicker and larger in extent as a result of increased baseflow. With permafrost degradation, potential changes in groundwater discharge may result in a changing pattern of icing occurrences.

7.1 Research implications and future work

The results of this study have implications for infrastructure planning as well as for future icing research. The resulting dataset provides important information for establishing new all-season roads to connect northern communities and possibly avoid geotechnical issues. However, close monitoring of icing development around road infrastructures still remains important. Updating the icing dataset with more recent imagery could help refine our findings. Moreover, the use of icing volume calculations done with an unmanned aerial vehicle (UAV) along with detailed hydrographic data could help better understand the relation between icings and local hydrology. As climate forecasts have multiple complex factors, making large-scale predictions of icing activity remains difficult. Thus, more in-depth investigations should be undertaken.

References

ÅKERMAN, J.H. (1982). Studies on naledi (icings) in west Spitsbergen. *Proc. 4th Canadian permafrost conference, Calgary, (National Research Council of Canada, Ottawa)*. pp. 189-202.

ALEKSEYEV, V. R,, (1973). Conditions Involved in Formation and Distribution of Naleds in Southern Yakutia. Siberian Naleds. V. R. Alekseyev (ed.), *CRREL Draft Translation* 399, pp, 43-58.

AYLSWORTH, J.M., BURGESS, M.M., DESROCHERS, D.T., DUK-RODKIN, A., ROBERTSON, T., and TRAYNOR, J.A., (2000). Surficial geology, subsurface materials, and thaw sensitivity of sediments; in The Physical Environment of the Mackenzie Valley, Northwest Territories: a base line for the assessment of Environmental Change, (ed) L.D. Dyke and G.R. Brooks; Geological Survey of Canada, *Bulletin 547*, p.41-48.

BENSE, V.F., FERGUSON, G., KOOI, H., (2009). Evolution of shallow groundwater flow systems in areas of degrading permafrost. *Geophysical Research Letters*, vol. 36, no. 22, L222401.

BENSE, V.F., KOOI, H., FERGUSON, G., READ, T., (2012). Permafrost degradation as a control on hydrogeological regimes shifts in a warming climate. *Journal of Geophysical Research: Earth Surface*, vol. 117, issue 3, article number F03036.

BRABETS, T.P., and WALVOORD, M.A., (2009). Trends in streaflow in the Yukon River Basin from 1944 to 2005 and the influence of the Pacific Decadal Oscillation. *Journal of Hydrology*, vol. 371, issue 1-4, p. 108-119.

BRING, A., DESTOUNI, G., (2011). Relevance of hydro-climatic change projection and monitoring for assessment of water cycle change in the arctic. *Ambio*, vol. 40, no. 4, pp. 361-369.

BUKAYEV, N, A., (1973). Basic Tendencies in Regime of Huge Naleds in Upper Reaches of Kolyma Diver Siberian Naleds. *CRREL Draft Translation* 399, Alekseyev, V. R. (ed.), Hanover, NH, pp. 92-11

BURN, C.R., KOKELJ, S.V. (2009). The environment and permafrost of the Mackenzie Delta area. *Permafrost and Periglacial Processes*, vol. 20, pp. 83-105.

CAREY, K. (1973). Icings Developed from Surface and Ground Water. *CRREL Monograph III-D3*.

CLARK, I. D., LAURIOL, B. (1997). Aufeis of the Firth River Basin, Northern Yukon, Canada: Insights into permafrost hydrogeology and karst. *Arctic and Alpine Research*, vol. 29, no. 2, pp. 240-252.

CLARK I.D., LAURIOL, B., HARWOOD L., & MARSCHNER, M. (2001). Groundwater contributions to discharge in a permafrost setting, Big Fish River, N.W.T., Canada. *Arctic and Antarctic Alpine Research* vol. 33, pp. 62–69.

COLBY, D.J. (1991). A review of assessing the accuracy of classifications of remotely sensed data. *Remote Sensing of the Environment*, vol. 37, pp. 35-46.

CONNON, R.F., QUINTON, W.L., CRAIG, J.R., & HAYASHI, M. (2014). Changing hydrologic connectivity due to permafrost thaw in the lower Liard River valley, NWT, Canada. *Hydrological Processes*, vol. 28, p. 4163-4178.

DEAN, K. G. (1984). Stream-icing zones in Alaska, Alaska Division. *Geophys. Surv. Rep. Invest*., 84-16, scale 1:250,000, Alaska Div. of Geol. and Geophys. Surv., Fairbanks.

DÉRY, S.J., and WOOD, E.F. (2005). Decreasing river discharge in northern Canada. *Geophyiscal Research Letters*, vol. 32, issue 10, 4 pp.

DOZIER, J. (1989). Spectral signature of alpine snow cover from the Landsat Thematic Mapper. *Remote Sensing of Environment*, vol. 28, pp. 9–22.

DUCHESNE, C., SMITH, S.L., EDNIE, M., & BONNAVENTURE, P.P., (2015). Active layer variability and change in the Mackenzie Valley, Northwest Territories. *Paper 117, IN GEOQuébec 2015*. (68th Canadian Geotechnical Conference and 7th Canadian Conference on Permafrost). Québec.

FOGA, S., SCARAMUZZA, P.L., GUO, S., ZHU, Z., DILLEY, R.D., BECKMANN, T., SCHMIDT, G.L., DWYER, J.L., HUGHES, M.J. & LAUE, B., (2017). Cloud detection algorithm comparison and validation for operational Landsat data products. *Remote Sensing of Environment*, vol. 194, pp. 379-390.

HALL, D. K., RIGGS, G. A., and SALOMONSON, V. V., (1995). Development of methods for mapping global snow cover using Moderate Resolution Imaging Spectroradiometer (MODIS) data, *Remote Sensing of Environment*, vol. 54, pp. 127–140.

HARDEN, D., BARNES, P., and REIMNITZ, E., (1977). Distribution and character of naleds in northeastern Alaska, *Arctic*, vol. 30, pp. 28–40.

HEGINBOTTOM, J.A. (2000). Permafrost distribution and ground ice in surficial materials. *Geological Survey of Canada, Bulletin 547*, pp. 31-39.

HUGHES, O.L., VEILLETTE, J.J., PILON, J., HANLEY, P.T. (1973). *Terrain evaluation with respect to pipeline construction, Mackenzie Transportation Corridor*. Environmental-Social Committee, Northern Pipelines, Taskforce on Northern Oil and Development, Report no. 73-37.

HU, X., POLLARD, W.H. (1997). The hydrologic analysis and modelling of river icing growth, North Fork Pass, Yukon Territory, Canada. *Permafrost and Periglacial Processes*, vol. 8, pp. 279-294.

St-JACQUES, J.M., and SAUCHYN, D.J., (2009). Increasing winter baseflow and mean annual streamflow from possible permafrost thawing in the Northwest Territories, Canada. *Geophysical Research Letters*, vol. 36, 6 pp.

KANE, D. L. and CARLSON, R. F., (1973). Hydrology of the Central Arctic River Basins of Alaska. *Institute of Water Resources, University of Alaska, Fairbanks, AK*, IWR-45, 51 pp.

KANE, D. L (1981). Physical mechanics of aufeis growth. *Canadian Journal of Civil Engineering*, vol. 8, issue 2, p. 186-195.

KANE, D.L., YOSHIKAWA, K., McNaMARA, J.P. (2013). Regional groundwater flow in an area mapped as continuous permafrost, NE Alaska (USA). *Hydrogeology Journal*, vol. 21, p. 41-52.

LABRECQUE, S., LACELLE, D., DUGUAY, C.R., LAURIOL, B., (2009*).* Contemporary (1951-2001) Evolution of Lakes in the Old Crow Basin, Northern Yukon, Canada : Remote Sensing, Numerical Modeling, and Stable Isotope Analysis. *Arctic*, vol. 62, no. 2., p.225-238.

LANTUIT H. and POLLARD WH. (2008) Fifty years of coastal erosion and retrogressive thaw slump activity on Herschel Island, southern Beaufort Sea, Yukon Territory, Canada. *Geomorphology* 95: 84–102. DOI:10.1016/j.geomorph.2006.07.040

LAPP, A., CLARK, I.D., MACUMBER, A.L., PATTERSON, T.R. (2017) Hydrology of the North Klondike River: Carbon export, water balance and inter-annual climate influences within a sub-alpine permafrost catchment. *Isotopes in Environmental and Health Studies*, vol. 53, no. 5, pp. 500-517.

LAURIOL, B., CINQ MARS, J., CLARK, I.D., (1991). Localisation, génèse et fonte de quelques naleds du nord du Yukon, (Canada). *Permafrost and Periglacial Processes*, vol. 2, pp. 225-236.

LIN, A, WANG, X.L. (2011). An algorithm for blending multiple satellite precipitation estimates with in-situ precipitation measurements in Canada. *Journal of Geophysical Research – Atmospheres*, vol. 116, no. D21, 19 pp.

MICHEL, F.A., (1986). Hydrogeology of the central Mackenzie Valley. *Journal of Hydrology*, vol. 85, pp.379-405.

McFEETERS, S. K. (1996). The use of the normalized difference water index (NDWI) in the delineation of open water features, *International Journal of Remote Sensing*, 17, pp. 1425–1432.

McCLELLAND, J.W., DERY, S.J., PETERSON, B.J., HOLMES, R.M., WOOD, E.F., (2006). A pan-arctic evaluation of changes in river discharge during the latter half of the 20th century. *Geophysical Research Letters*, vol. 33, L06715.

McNAMARA, J.P., KANE, D.L., HINZMAN, L.D., (1998). An analysis of streamflow hydrology in the Kuparuk River Basin, Arctic Alaska; a nested watershed approach. *Journal of Hydrology*, vol. 206, p.39-57.

MUTCH, R.A., McCART, P.J. (1974). Springs within the northern Yukon drainage system (Beaufort Sea drainage). Chapter IX, Canadian Arctic Gas Study Limited, Alaskan Arctic Gas Study Co., *Arctic Gas Biological Report* 15: 36 p.

NEKRASOV, I.A., (1969). Naleds in Eastern part of Stanovote upland. *In collection : Naledi Sibiri (Naleds of Siberia)*. Moscow, Nauka (Science Press).

OMELON, C.R., POLLARD, W.H., ANDERSEN, D.T., (2005). A geochemical evaluation of perennial spring activity and associated mineral precipitates at Expedition Fjord, Axel Heiberg Island, Canadian High Arctic. *Applied Geochemistry*, vol. 21, issue 1, p. 1-15.

PASTICK, N.J., JORGENSON, M.T., WYLIE, B.K., NIELD, S.J., JOHNSON, K.D., FINLEY, A.O., (2015). Distribution of near-surface permafrost in Alaska; Estimates of present and future conditions. *Remote sensing of Environment*, vol. 168, p. 301-315.

PAVELSKY, T.M., ZARNETSKE, J.P. (2017). Rapid decline in river icings detected in Arctic Alaska: Implications for a changing hydrologic cycle and river ecosystems. *Geophysical Research Letters*, vol. 44, issue 7, p. 3228-3235.

POLLARD, W.H., FRENCH, H.M., (1984). The groundwater hydraulics of seasonal frost mounds, North Fork Pass, Yukon Territory. *Canadian Journal of Earth Sciences*, vol.21, p. 1073-1081.

POLLARD, W. H. and van EVERDINGEN, R. O. (1992). Formation of seasonal ice bodies. In Dixon, J. C. and Abrahams, A. D. (ed.), *Periglacial Geomorphology*. Wiley, pp. 281-304.

POLLARD, W.H., OMELON, C., ANDERSEN, D., MCKAY, C. (1999). Perennial spring occurrence in the Expedition Fiord area of western Axel Heiberg Island, Canadian High Arctic. *Canadian Journal of Earth Sciences*, vol. 36, no. 1, pp.105-120.

POLLARD, W.H. (2005) Icing processes associated with high arctic perennial springs, Axel, Heiberg Island, Nunavut, Canada. *Permafrost and Periglacial Processes*, vol. 16, pp.51-68.

PROKOPH, A., ADAMOWSKI, J., ADAMOWSKI, K., (2012) Influence of the 11-year solar cycle on annual streamflow maxima in Southern Canada. Journal of Hydrology, vol., 442-443, p. 55-62.

RIORDAN, B., VREBYL, D., McGUIRE, A.D., (2006) Shrinking ponds in subarctic Alaska based on 1950-2002 remotely sensed images. *Journal of Geophysical Research: Biogeosciences*, vol. 111, no. 4, G04002.

SMITH, S.L., RISEBOROUGH, D.W., BONNAVENTURE, P.P., DUCHESNE, C., (2016) *An ecoregional assessment of freezing season air and ground surface temperature in the Mackenzie Valley corridor, NWT, Canada*. Cold Regions Science and Technology, vol. 125, p. 152-161.

SMITH, S.L., CHARTRAND, J., DUCHESNE, C., and EDNIE, M., (2017) Report on 2015 field activites and collection of ground thermal and active layer data in the Mackenzie corridor, Northwest Territories. *Open file* 8125, Geological Survey of Canada, 133 pp.

SMITH, S.L., CHARTRAND, J., DUCHESNE, C., and EDNIE, M., (2017) Report on 2016 field activites and collection of ground thermal and active layer data in the Mackenzie corridor, Northwest Territories. *Open file* 8303, Geological Survey of Canada, 102 pp.

SPENCE, C., KOKELJ, S.V., EHSANZADEH, E. (2011) Precipitation trends contribute to streamflow regime shifts in northern Canada. Symposium H02 on Cold Regions Hydrology in a Changing Climate, Held During the 25th General Assembly of the International Union of Geodesy and Geophysics, IUGG 2011; Melbourne, VIC; Australia; 28 June 2011 through 7 July 2011; Code 89593.

STERLING, H. (1935). Winter problems on Alaskan roads. *Roads and Streets*, vol. 78, p. 399-400

STEVENS, J.C. (1940). Winter overflow from ice-gorging on shallow streams. *Transactions of the American Geophysical Union*, vol. 21. p. 973-97.

STUART, R.A., JUDGE, A.S. (1991). On the applicability of GCM estimates to scenarios of global warming in the Mackenzie Valley area. *Climatological Bulletin*, vol. 25, pp. 147-169.

STUART, R.A., ETKIN, D.A., JUDGE, A.S. (1991). Recent observations of air temperature and snow depth in the Mackenzie Valley area and their implications on the stability of permafrost layers. Environment Canada, Atmospheric Environment Service, Canadian Climate Centre, Report no. 91-2, 178p.

SOKOLOV, B.L. (1974). Estimation of the naled component in genetic separation of the hydrograph of rivers in the permafrost zone. *Sov Hydrol*, Issue 4, p.215-228.

TARNOCAI, C., NIXON, F.M., KUTNY, L. (2004). Circumpolar Active Layer Monitoring (CALM) Sites in the Mackenzie Valley, Northwestern Canada. *Permafrost and Periglacial Processes*, vol. 15, pp. 141-153.

TAYLOR, I.P. (1939). Road maintenance in Alaska. *Pacific Builder and Engineer,* vol. 45, no. 31, p. 36.

THOMSON, S. (1966). Icings on the Alaska Highway. Proceedings, International Conference on Permafrost, 11-15 Nov 1963, Lafayette, Indiana; National Academy of Sciences, National Research Council, Washington, p. 526-529.

VAN EVERDINGEN, R.O., (1981). Morphology, hydrology and hydrochemistry of karst in permafrost terrain near Great Bear Lake, Northwest Territories. *Science Series*, no. 114.

VEILLETTE, J. J., and THOMAS R.D., (1979). Icings and seepage in frozen glaciofuvial deposits, District of Keewatin, N.W.T., *Canadian Geotechnical Journal*, vol 16, issue 4, pp. 789-798.

VERMOTE, E., JUSTICE, C., CLAVERIE, M., FRANCH, B., (2016) Preliminary analysis of the performance of the Landsat land surface reflectance product. *Remote Sensing of Environment*, vol. 185, p. 46-56.

UTTING, N., LAURIOL, B., MOCHNACZ, N., AESCHBACH-HERTIG, W., CLARK, I. (2013) Noble gas and isotope geochemistry in western Canadian Arctic watersheds: tracing groundwater recharge in permafrost terrain. *Hydrogeology Journal*, vol. 21, issue 1, pp. 79-91.

WAINSTEIN, P., MOORMAN, B., WHITEHEAD, K., (2014) Glacial conditions that contribute to the regeneration of Fountain Glacier proglacial icing, Bylot Island, Canada. *Hydrological Processes*, vol. 28, no. 5, p. 2749-2760.

WALVOORD, M.A., STRIEGL, R.G. (2007). Increased groundwater to stream discharge from permafrost thawing in the Yukon River basin: Potential impacts on lateral export of carbon and nitrogen. *Geophysical Research Letters*, vol. 34, L12402, doi:10.1029/2007GL030216.

WALVOORD, M.A., CLIFFORD, I.V., WELLMAN, T.P. (2012). Influence of permafrost distribution on groundwater flow in the context of climate-driven permafrost thaw : Example from Yukon Flats Basin, Alaska, United States. *Water Resources Research*, vol. 48, W07524, doi:10.1029/2011WR011595

WANTY, R.B., WANG, B., VOHDEN,J., DAY, W.C., GOUGH, L.P., (2010) Aufeis accumulations in stream bottoms in arctic and subarctic environments as a possible indicator of geologic structure. In: GOUGH, L.P., DAY, W.C., (eds) 2010, Recent US Geological Survey studies in the Tintina Gold Province, Alaska, United States, Yukon, Canada: results of a 5-year project. *US Geological Survey Science Invest Report* 2007-5289.

WASHBURN, L. A. (1979). Geocryology. *A survey of periglacial processes and environments.* E. Arnold, London, 406 pp.

WILIAMS, J.R., VAN EVERDINGEN, R.O. (1973) Groundwater investigations in permafrost regions of North America; a review. Permafrost : North American Contribution, Second International Conference, Washington, D.C.; National Academy of Sciences, pp.435-446.

WOO, M.K., (2012) Permafrost Hydrology (book), Springer-Verlag, Berlin. DOI 10.1007/978-3-642-23462-0

WRANGEL, F. P. (1841). Puteshes tviya k severnym beregam Sibiri i po Ledovitomu moryu sovershennyye 1820-1824 gg. (A journey to the northern shores of Siberia and along the Arctic Oceal) made in 18 20-1824). Text in Russian. St. Petersburg.

YOSHIKAWA, K., HINZMAN, L.D., KANE, D.L. (2007). Spring and aufeis (icing) hydrology in Brooks Range, Alaska. *Journal of Geophysical Research*, vol. 112, issue G04S43.

YOUNG, N.E., ANDERSON, R.S., CHIGNELL, S.M., VORSTER, A.G., LAWRENCE, R., EVANGELISTA, P.H. (2017) A survival guide to Landsat preprocessing. *Ecology*, 98, (4), pp.920-932.

ZHANG, X., VINCENT, L.A., HOGG, W.D., and NIITSOO, A., (2000) Temperature and precipitation trends in Canada during the 20th century. *Atmosphere-Ocean*, vol. 38, issue 3, p.395-429.

ZHU, X., L. DESHENG, J. CHEN (2012), A new geostatistical approach for filling gaps in Landsat ETM+ SLC-off images, *Remote Sensing of Environment*,124, 49–60, doi:10.1016/j.rse.2012.04.019.

ZOLTAI, S.C., TAYLOR, S., JEGLUM, J.K., MILLS, G.F. and JOHNSON, J.D. (1988) Wetlands of boreal Canada. *In*: Wetlands of Canada. Ecological Land Classification Series No. 24, *Environment Canada and Polysciences Publications*, pp.98-154

Appendix A

Python Scripts

```
from __future__ import division
import os
import arcpy
from arcpy.sa import *
from arcpy import env
env.overwriteOutput=True
arcpy.CheckOutExtension("spatial")
rootfolder=r'F:\Hugo_aufeis\57_14'
for root, dirs, files in os.walk(rootfolder):
    for d in dirs:
        band2 = Raster(rootfolder + os.sep + d + os.sep + d + "_sr_band2.tif")
        band4 = Raster(rootfolder + os.sep + d + os.sep + d + "_sr_band4.tif")
        band7 = Raster(rootfolder + os.sep + d + os.sep + d + "_sr_band7.tif")
        composite = arcpy.CompositeBands_management([band7,band4,band2],rootfolder+os.sep+d+os.sep+d+"_composite.tif")
```

Script for creating false-color composite (7,4,2)

```
from __future__ import division
import arcpy
from arcpy.sa import *
import os
from arcpy import env
arcpy.CheckOutExtension("spatial")
env.overwriteOutput=True
rootfolder=r'F:\Hugo_aufeis\57_14'
for root, dirs, files in os.walk(rootfolder):
    for d in dirs:
        b2 = rootfolder+os.sep+d+os.sep+d+"_sr_band2.tif"
        b5 = rootfolder+os.sep+d+os.sep+d+"_sr_band5.tif"
        band2 = Raster(b2)
        band5 = Raster(b5)
        NDSI=(band2-band5)/(band2+band5)
        NDSI.save(rootfolder+os.sep+d+os.sep+d+"_NDSI.tif")
        NDSI_tresh=NDSI>=0.4
        NDSI_tresh.save(rootfolder+os.sep+d+os.sep+d+"_NDSI_tresh0.4.tif")
```

Script for Normalized Difference Ice Index (NDSI)

```
from __future__ import division
import os
import arcpy
from arcpy.sa import *
from arcpy import env
arcpy.CheckExtension("spatial")
env.overwriteOutput=True
rootfolder=r'F:\Hugo_aufeis\57_14'
for root, dirs, files in os.walk(rootfolder):
    for d in dirs:
        MDII=Raster(rootfolder+os.sep+d+os.sep+d+"_MDII.tif")
        MDII_div=MDII/100000
        MDII_div.save(rootfolder+os.sep+d+os.sep+d+"_MDII_div.tif")
```

Script for Maximum Difference Ice Index (MDII)

```
from __future__ import division
import arcpy
from arcpy.sa import *
import os
from arcpy import env
arcpy.CheckOutExtension("spatial")
env.overwriteOutput=True

rootfolder=r'Z:\63_15'
for root, dirs, files in os.walk(rootfolder):
    for d in dirs:
        b2 = rootfolder+os.sep+d+os.sep+d+"_sr_band2.tif"
        b4 = rootfolder+os.sep+d+os.sep+d+"_sr_band4.tif"
        band2 = Raster(b2)
        band5 = Raster(b4)
        NDSI=(band2-band4)/(band2+band4)
        NDSI.save(rootfolder+os.sep+d+os.sep+d+"_NDWI.tif")
```

Script for NDWI

Appendix B

Details of attributes from the *icing_point.shp* shapefile dataset.

Attribute field	***Description***
OBJECTID	Random numbering assigned by ArcGIS
x_utm	X UTM coordinates (zone 8N)
y_utm	Y UTM coordinates (zone 8N)
x_dd	X coordinates (decimal degrees)
y_dd	Y coordinates (decimal degrees)
CDEM	Value of elevation from CDEM below icing point, in meters
REGION_NAME	Ecoregion name
CDEM_slope	Value of slope (degrees, calculated from CDEM) underneath icing point
UTYPE1	Surficial geology type found below icing point (data from Canadian Geoscience Map 195)
PMF_CLASS	Permafrost class found below icing centroid (spatial data from GSC Bulletin 548, E=extensive discontinuous, C = continuous)
ROCK_MAJOR YUKON	Parent bedrock found below icing crentroid in YT (Yukon Digital Bedrock Geology, 2018 update)
MajorLith	Parent bedrock found below icing centroid in N.W.T. (data from N.W.T. Open File 201609)
WSCSSDANAM	National Hydro Network watershed (level 3) name found below icing point
name_en	Name of river/stream closest to icing point (dataset from CanVec 1:1 000 000 water course line shapefile)
NEAR_FAULTS_M	Distance in meters to the closest geological fault (N.W.T. OF201609 and Yukon Geological Survey Bedrock Geology dataset)
NEAR_PMF_LIMIT_KM_1	Distance in kilometers of icing point to the southern continuous permafrost limit (based on GSC Bulletin 548 data)

Number of Landsat 5 and 7 scenes used for analysis.

(WRS1)		
Path_row	Landsat 5	Landsat 7
51_15	16	0
52_15	17	10
52_16	7	8
53_16	16	0
54_14	17	13
54_15	18	12
54_16	0	2
55_14	18	0
55_15	12	0
55_16	10	0
57_13	20	12
57_14	16	11
57_15	9	5
57_16	6	5
58_13	15	0
58_14	10	0
58_15	9	0
60_12	17	12
60_13	17	11
60_14	10	3
60_15	8	5
62_11	0	12
62_12	18	0
62_13	16	0
62_14	11	0
62_15	11	0
63_11	10	15
63_12	20	14
63_13	11	11
63_14	9	8
63_15	6	6
65_12	11	0
65_13	7	0
total	398	175
	Total = 573	